photonics

MDPI

Review

Chalcogenide Fiber and Microcavity Platforms for Mid-Infrared Sensing and Nonlinear Photonics

Chenyue Xiao and Xiaosong Lu *

Jiangsu Key Laboratory of Advanced Laser Materials and Devices, School of Physics and Electronic Engineering, Jiangsu Normal University, Xuzhou 221116, China; chenyue_xiao@mymail.sutd.edu.sg

* Correspondence: xingwadyx@jsnu.edu.cn

Abstract

Chalcogenide glasses are versatile mid-infrared (MIR) photonic materials because they combine broad infrared transparency, high refractive index, strong third-order nonlinearity, and processability into fibers, microfibers, planar waveguides and microcavities. This review examines chalcogenide fiber, waveguide, and microcavity platforms for MIR sensing and nonlinear photonics from a system-level perspective. We discuss material families, processing routes and device-relevant loss mechanisms; review fiber evanescent-wave spectroscopy, structured and functionalized fiber probes, microfibers, planar waveguides, resonators and suspended high-overlap waveguide sensors; and analyze nonlinear and active chalcogenide fibers and high-Q microcavities as MIR source platforms. Emphasis is placed on the transition from single-pass evanescent absorption to Q–overlap co-design and from isolated component demonstrations to source–waveguide–cavity–sensor–detector integration for compact molecular spectroscopy.

Keywords: chalcogenide glasses; mid-infrared photonics; fiber evanescent-wave spectroscopy; cavity-enhanced sensing; optical microcavities; supercontinuum generation; Kerr microcombs; integrated photonic sensors

1. Introduction

Chalcogenide glasses provide one of the most versatile material bases for compact mid-infrared (MIR) photonics. Their broad infrared transparency, high refractive index, large third-order optical nonlinearity, and glass-forming flexibility allow them to be processed into fibers, microfibers, thin-film waveguides, optical resonators and nonlinear photonic devices [1–6]. Within this family, sulfide, selenide and telluride glasses cover different MIR windows and offer different balances among transparency, thermal stability, nonlinear response and processability [5–10]. Hybrid-integrated chalcogenide photonics have further expanded the field from bulk and fiber optics toward wafer-scale thin-film circuits, resonators and heterogeneous photonic integration [11].

The importance of chalcogenide platforms has increased with the broader development of MIR-integrated photonics and molecular sensing. Recent work on MIR photonic circuits, waveguide spectroscopy, chem/bio sensing, and advanced infrared sensor systems has shifted the field from isolated waveguides or resonators toward complete spectroscopic architectures [12–20]. In practical MIR sensing, analytical performance is not determined by a single figure of merit such as propagation loss, resonator quality factor, or spectral bandwidth. It depends on the combined behavior of the light source, delivery waveguide, sensing interface, optical transducer, detector, calibration method and package environment.

Received: 21 July 2026
Revised: 7 September 2026
Accepted: 14 September 2026
Published: 22 September 2026

Sample delivery, surface chemistry, water or matrix background, detector noise, baseline drift and thermal stability can therefore be as important as the nominal optical loss of the chalcogenide component itself.

Early chalcogenide MIR sensing was driven by fiber evanescent-wave spectroscopy (FEWS). In FEWS, an infrared-transmitting fiber acts both as a light-delivery path and as a chemically interactive interface. Foundational studies demonstrated remote fiber-optic chemical sensing and infrared evanescent absorption spectroscopy using chalcogenide and telluride glass fibers [21,22]. These works established chalcogenide fibers as MIR sensing probes, while also revealing persistent constraints: single-pass interaction, limited evanescent-field fraction, water background, surface fouling, fiber fragility, and reliance on external sources and detectors. These limitations motivated the transition from simple exposed fibers toward structured probes, compact MIR source technology, microfibers, resonant fiber devices, and integrated waveguide sensors.

This evolution has produced several complementary chalcogenide device classes. Structured and functionalized fiber probes, including tapered, side-polished, ring-shaped, helical and surface-modified fibers, increase the accessible evanescent field or improve local interaction with the analyte. Chalcogenide microfibers and fiber-integrated resonators provide stronger field exposure, wavelength selectivity, and fiber-compatible resonant enhancement. Planar chalcogenide waveguides and microcavities add lithographic control, compact sensing geometries, high-Q resonances, and compatibility with microfluidic or detector integration. In parallel, nonlinear chalcogenide fibers and microcavities provide broadband, tunable, coherent or narrow-linewidth MIR source functions through supercontinuum generation, four-wave mixing, optical parametric conversion, Kerr comb generation, and Brillouin lasing. Selected active doped chalcogenide sources are considered only as related MIR source options where they clarify source selection for sensing. Chalcogenide glasses should therefore be viewed not only as passive infrared-transmitting media but as multifunctional platforms that can support light generation, delivery, molecular interaction, resonant enhancement and readout.

The conceptual evolution of chalcogenide MIR photonics is summarized in Figure 1. The figure follows the field from fiber-based evanescent-wave sensing to structured and functionalized fiber probes, microfibers, planar waveguides, microcavities, nonlinear MIR sources, and integrated source–sensor–detector architectures. This progression also defines the structure of the present review: material properties first enable MIR transmission and nonlinearity; device geometry then controls field exposure, resonant enhancement and dispersion; and system integration finally determines whether these advantages can be translated into stable molecular sensing.

This review examines chalcogenide fibers, waveguides, microcavities and source devices as connected components of a unified MIR photonic platform. The focus is not simply on achieving lower loss, higher Q factor, or broader nonlinear spectra as isolated records. Instead, we emphasize how material transparency, waveguide confinement, cavity enhancement, nonlinear source generation, detector integration, and sample handling can be combined to produce stable, selective, and deployable MIR sensing systems. Related active doped chalcogenide sources are included only as boundary-setting examples of band-specific MIR source options. This source–waveguide–cavity–sensor–detector perspective is particularly important for chalcogenide photonics because the same material family can provide flexible delivery fibers, high-overlap sensing interfaces, resonant enhancement structures, and compact MIR source functions.

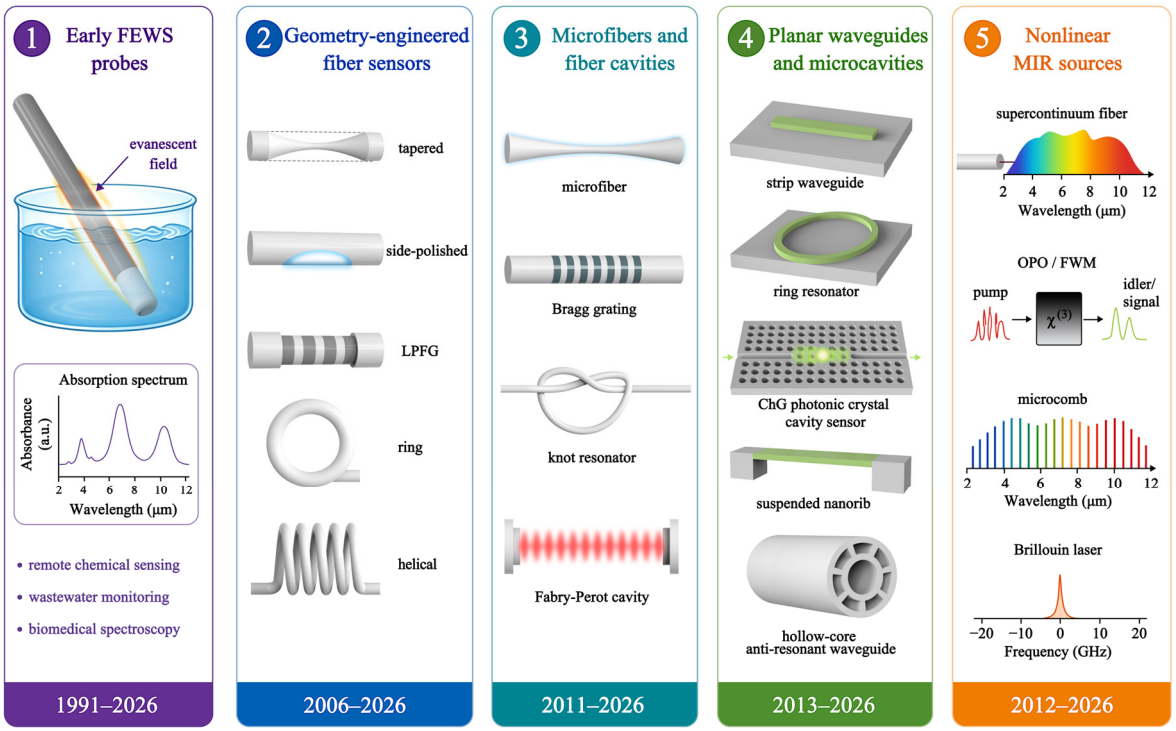

Figure 1. Evolution of chalcogenide MIR photonic platforms from fiber evanescent-wave sensing to integrated source–sensor–detector systems. The figure summarizes the transition from early FEWS probes, structured and functionalized fiber probes and chalcogenide microfibers to planar waveguides, microcavities, nonlinear MIR sources, and integrated source–sensor–detector architectures.

The review is organized into six sections. Section 2 summarizes material foundations, processing routes and device-relevant loss mechanisms. Section 3 reviews chalcogenide fiber, microfiber, planar-waveguide, and microcavity platforms for MIR sensing. Section 4 discusses chalcogenide source platforms for MIR sensing and nonlinear photonics, with active doped-fiber sources treated only as related source options. Section 5 addresses integrated source–sensor–detector systems and application-driven design rules. Section 6 concludes by identifying practical routes toward deployable chalcogenide MIR photonic systems.

2. Material Foundations, Processing, and Device-Relevant Loss Mechanisms

Chalcogenide glasses are defined by networks based on sulfur, selenium or tellurium, often combined with network-forming or modifying elements such as As, Ge, Sb, Ga and Te. Their value for mid-infrared (MIR) photonics arises from the combination of broad infrared transparency, high refractive index, large optical nonlinearity, compositional flexibility and compatibility with fiber, thin-film and resonator platforms. These advantages make them suitable for evanescent-wave sensing, planar waveguide spectroscopy, nonlinear frequency conversion, supercontinuum generation, Kerr comb formation, and Brillouin lasing.

However, the material properties that make chalcogenide glasses attractive also introduce device-level constraints. High refractive index enables tight confinement but increases sensitivity to roughness, coupling mismatch and surface scattering. Broad MIR transparency is useful only if impurity absorption, surface contamination, substrate absorption, and packaging-related loss are controlled. Large Kerr nonlinearity reduces nonlinear thresholds, but practical performance still depends on propagation loss, coupling efficiency, dispersion accuracy and thermal stability. Therefore, chalcogenide MIR platforms should

be evaluated through a combined material, fabrication and system-integration framework rather than by bulk transparency alone.

Recent MIR photonic and sensing studies provide the broader platform context in which chalcogenide devices should be evaluated. Integrated MIR photonics has moved toward compact source–waveguide–sensor–detector architectures, where transparency, confinement, coupling, dispersion, and packaging must be optimized together rather than separately [12–15]. Thin-film MIR waveguide platforms further show that chip-scale spectroscopy is governed not only by material absorption, but also by waveguide geometry, analyte overlap, propagation loss and interface stability [16,17]. In parallel, fiber-optic MIR sensing studies emphasize flexible delivery, remote operation, and long interaction length but also expose persistent limitations associated with background absorption, surface contamination, bending loss, and sample contact reproducibility [18]. Recent chem/bio sensing and advanced MIR sensor reviews further clarify that practical molecular detection requires the co-design of optical platform, sample interface, spectral readout and environmental stabilization [19,20]. These broader studies define the system-level requirements that chalcogenide fibers, waveguides, and microcavities must satisfy.

2.1. Material Families and Structure–Property–Function Relations

Sulfide, selenide and telluride glasses provide different balances among MIR transparency, processability, nonlinearity and device stability. Sulfide glasses such as As_2S_3, Ge–As–S and Ge–Sb–S are attractive in the short- to mid-infrared because they combine relatively mature processing, good thermal stability, high refractive index, and compatibility with fiber, thin-film and microresonator fabrication. Selenide glasses such as As_2Se_3, Ge–As–Se and Ge–Sb–Se extend the useful transmission window toward longer wavelengths and generally provide higher optical nonlinearity, making them especially valuable for deeper-MIR sensing, nonlinear fibers, suspended-core structures, and integrated waveguides. Telluride glasses can access still longer wavelengths, but their practical use is more strongly constrained by purification difficulty, crystallization tendency, narrow thermal-processing windows and mechanical reliability [5,6,10].

Material selection should therefore begin from the target wavelength, device geometry, and operating environment rather than from the widest nominal bulk transparency window. For sensing and nonlinear photonics around 2–5 μm, sulfide and Ge–Sb–S systems remain attractive because they support compact waveguides, microresonators, and fiber-format devices with comparatively mature processing. Beyond 5 μm, selenide and Ge–Sb–Se glasses become increasingly important because of their broader MIR transparency and stronger nonlinearity. For long-wave MIR operation approaching 8–12 μm, telluride or long-wave selenide systems may be required. However, a broader nominal transparency window does not automatically lead to a better device. If purification, drawing, coating, polishing, etching or packaging cannot preserve low loss at the operating wavelength, a theoretically broader glass may underperform a more mature sulfide or selenide platform.

The transition from selenium- to tellurium-based chalcogenide fibers illustrates this device-level trade-off [10]. Selenium-based glasses provide broader MIR transmission than sulfides and have been widely used in nonlinear fibers, suspended-core fibers, and integrated waveguides. Tellurium-based glasses can further extend the operating wavelength, but they are more sensitive to crystallization, impurity absorption and mechanical degradation. Material choice is therefore not a simple ranking of bulk transparency; it is a system-level decision that depends on the required wavelength range, optical loss, mechanical robustness, fabrication route, and package environment.

The relationships among chalcogenide material families, device formats, and MIR photonic functions are summarized in Table 1. The table uses broad material, integrated

photonics, waveguide spectroscopy, and chem/bio sensing references to position chalcogenide fibers, planar waveguides, and microcavities within the wider MIR device landscape [5,6,10–20]. More specific sensing and nonlinear-source demonstrations are discussed in Sections 3 and 4.

Table 1. Representative chalcogenide material families and device platforms for MIR sensing and nonlinear photonics.

Category	Representative Compositions or Platforms	Main Advantages	Main Limitations	Suitable MIR Functions
Sulfide glasses	As_2S_3, Ge–As–S, Ge–Sb–S	Relatively mature processing; good thermal stability; high refractive index; compatibility with fibers, thin films and resonators	Shorter long-wavelength cutoff than selenide and telluride glasses; impurity and surface absorption remain important	FEWS fibers; planar waveguides; microcavities; short- to mid-MIR nonlinear devices [5,6,11]
Selenide glasses	As_2Se_3, Ge–As–Se, Ge–Sb–Se	Broader MIR transparency than sulfides; generally higher third-order nonlinearity; useful for deeper-MIR operation	More sensitive to impurity absorption, surface quality and processing conditions	Long-wave FEWS; nonlinear fibers; suspended-core fibers; integrated MIR waveguides; nanorib gas sensors [5,6,10,11]
Telluride glasses	Ge–As–Te, Ge–Sb–Te and Te-rich chalcogenide glasses	Access to longer MIR wavelengths; potential for long-wave sensing and nonlinear devices	Purification difficulty; crystallization tendency; narrow processing window; weaker mechanical robustness	Long-wave MIR fibers; shaped probes; specialty sensing platforms [10]
Fiber platforms	Step-index, tapered, side-polished, suspended-core, helical and photonic crystal fibers	Flexible delivery; long interaction length; compatibility with remote sensing and nonlinear generation	Drawing loss, bending loss, coating absorption, fragility, and reproducible sample contact	FEWS; environmental sensing; biomedical probes; SCG; FWM; Raman and parametric sources [5,6,10,18–20]
Planar waveguides	Strip, rib, slot, subwavelength-grating, suspended nanorib and hollow-core/ARROW-type structures	Compact routing; lithographic control; compatibility with microfluidics, gas cells and detector integration	Thin-film stress, etching loss, sidewall roughness, process residues, coupling loss, and packaging complexity	On-chip absorption spectroscopy; high-overlap gas sensing; integrated source–sensor circuits [11–17,19,20]
Microcavities	Ring resonators, disks, WGM cavities, photonic-crystal cavities and Fabry–Perot cavities	Resonant enhancement; small footprint; high spectral selectivity; reduced nonlinear threshold	Q–overlap trade-off; thermal drift; coupling sensitivity; surface adsorption; substrate and cladding absorption	Cavity-enhanced sensing; Kerr combs; Brillouin lasers; nonlinear oscillators [11–15,19,20]

A recurring distinction in chalcogenide photonics is the gap between nominal bulk transparency and practical device loss. Bulk glasses may transmit broadly in the infrared, whereas fibers, waveguides and resonators are additionally limited by residual impurity

absorption, surface contamination, scattering, substrate absorption, process residues and environmental adsorption. Hydrogen-, oxygen-, carbon- and water-related bonds can introduce absorption bands in the same spectral region used for molecular sensing. In fibers, these impurities reduce signal-to-noise ratio and nonlinear conversion efficiency. In microfibers, surface adsorption and mechanical perturbation become more severe because the optical field is strongly exposed. In high-Q microcavities, even weak absorption from moisture, airborne molecules, or residual processing species can substantially degrade resonator performance.

The high refractive index of chalcogenide glasses is also a double-edged advantage. It enables tight confinement, small mode areas, strong evanescent-field engineering, and compact resonators, which are beneficial for sensing and nonlinear optics. At the same time, high index contrast increases sensitivity to sidewall roughness, facet reflection, coupling mismatch and surface-induced scattering. A highly confined waveguide is therefore not necessarily the best sensor if analyte overlap is weak, coupling drift is large, or surface loss dominates the measurement.

Large third-order nonlinearity is another defining feature of chalcogenide platforms. In fibers and microfibers, it enables supercontinuum generation, four-wave mixing, Raman scattering, and parametric conversion. In microcavities, high nonlinearity combined with high Q and small mode volume enables Kerr comb generation and Brillouin lasing. These nonlinear functions address a central system bottleneck in MIR spectroscopy: the need for compact broadband, tunable or narrow-linewidth sources that can be integrated with sensing and detection modules.

The material basis of chalcogenide MIR photonics is therefore best understood through a structure–property–function–loss framework. The transparency window determines which molecular bands can be accessed. The refractive index determines confinement, evanescent overlap, and coupling. The nonlinear coefficient determines source-generation efficiency. Impurities, surface quality, fabrication residues, substrate choice, and packaging determine the usable device window. This framework allows fibers, microfibers, planar waveguides, and microcavities to be compared within a common MIR photonic platform.

Overall, material selection in chalcogenide MIR photonics should be treated as a device-level and system-level decision. Sulfide, selenide, and telluride glasses offer different balances among transparency, processability, nonlinearity, stability, and loss. These trade-offs determine whether a given composition is better suited to fiber sensing, nonlinear source generation, planar microcavities, or hybrid source–sensor–detector integration.

2.2. Processing, Coupling, Packaging, and Stability

Device performance in chalcogenide MIR photonics is determined not only by glass composition, but also by how the material is converted into a fiber, waveguide, or cavity. In fiber platforms, the relevant factors include preform purity, drawing stability, core–cladding geometry, coating, surface condition, and post-drawing handling. Step-index fibers are comparatively mature, whereas suspended-core and photonic-crystal fibers provide stronger dispersion and evanescent-field control but require more demanding fabrication. Microfibers and microwires further increase this difficulty because reduced diameter strengthens surface-field exposure while also increasing mechanical fragility, bending loss, and sensitivity to surface contamination. A device optimized for evanescent interaction or nonlinear confinement can therefore fail at the system level if it cannot be handled, cleaned, packaged, or coupled reproducibly.

Planar chalcogenide devices introduce a different but related set of processing constraints. Thin films prepared by thermal evaporation, sputtering, pulsed-laser deposition, or related methods must maintain appropriate stoichiometry, density, stress, thickness

uniformity, and surface roughness. Lithography and etching then determine sidewall morphology, waveguide width accuracy, resonator roundness, and coupling-gap reproducibility. These factors are especially important in the MIR because post-etch residues, rough sidewalls, polymer residues, fluoropolymer claddings, or incomplete cleaning can introduce absorption or scattering in the same spectral region targeted for molecular sensing. Thus, propagation loss and resonator Q are not simply material parameters; they are outcomes of the complete deposition–patterning–etching–cleaning sequence.

The hybrid-integrated GeSbS platform provides a useful example of this process-to-device connection [11]. In that work, wafer-scale GeSbS films were deposited at low temperature, annealed to reduce surface roughness, patterned by electron-beam lithography, and transferred into waveguides through optimized dry etching. The reported process evidence includes a 4-inch GeSbS wafer, film thickness and refractive index uniformity maps, roughness reduction after annealing, vertical sidewalls after etch optimization, high-Q microresonators, and long spiral waveguides. This type of fabrication-level demonstration is important for a review because it connects intrinsic material properties, such as transparency, Kerr nonlinearity, and damage threshold with device metrics such as propagation loss, Q factor, dispersion accuracy, and nonlinear threshold.

Coupling remains a major bottleneck for both sensing and nonlinear devices. The high refractive index of chalcogenide glasses enables tight confinement and small mode area, but it also creates mode mismatch and Fresnel reflection at facets. End-fire coupling is straightforward but alignment-sensitive. Inverse tapers and mode converters can reduce coupling loss but add fabrication complexity and may introduce new process tolerances. Grating couplers can simplify wafer-scale testing, but their bandwidth, polarization tolerance, and MIR efficiency are often limited. In resonator sensors, coupling determines the loaded Q factor, extinction ratio, and linewidth. In nonlinear sources, coupling loss raises the effective threshold and reduces usable output power. Coupling design should therefore be treated as part of the device architecture rather than as an external measurement issue.

Packaging is particularly challenging because sensing and protection impose conflicting requirements. The optical field must interact with the target gas, liquid or surface-bound analyte, but the device must also be protected from water vapor, dust, organic residues, mechanical perturbation, and uncontrolled ambient adsorption. Many polymers, adhesives and encapsulants absorb strongly in the MIR and cannot be placed close to the optical mode without adding parasitic loss. Microfluidic channels, gas cells, windows, spacers and sealants must therefore be designed together with the optical mode distribution. For practical sensing systems, selective exposure of the sensing region, reference channels, passivation layers, dry-gas purging, differential readout, and replaceable sample interfaces may be as important as waveguide loss or cavity Q.

Thermal and environmental stability provide another device-level constraint. High-Q resonators are highly sensitive to small temperature changes, and nonlinear microcavities require stable pump–resonance detuning. In sensing, thermal resonance shifts can mimic refractive-index changes or absorption-induced linewidth variations. In fibers and microfibers, bending, contact pressure, humidity, and surface adsorption can alter the baseline response. For field-deployable MIR sensors, passive robustness, reference correction, temperature control, and packaging stability may therefore matter more than the highest laboratory Q factor or the lowest loss measured under ideal conditions.

These factors form a device-level loss chain that includes impurity absorption, sidewall roughness, process residues, surface-adsorbed molecules, substrate or cladding absorption, packaging-induced MIR absorption, and thermal drift. This chain determines whether the intrinsic advantages of chalcogenide glasses—broad MIR transparency, high refractive index, and large optical nonlinearity—can be translated into stable sensing, nonlinear gener-

ation or integrated source–sensor–detector operation. The central engineering requirement is therefore co-design: material purification, waveguide geometry, the fabrication process, coupling scheme, sample interface, and package environment must be optimized together.

This material and processing discussion provides the design basis for the sensing platforms reviewed below. In FEWS and microfiber probes, the decisive material properties are not only MIR transparency but also surface stability, mechanical robustness, and controllable evanescent-field exposure. In planar resonators and suspended waveguides, the same glass properties must be translated into low-loss confinement, reproducible coupling, stable Q-overlap balance, and MIR-compatible packaging. Section 3 therefore treats sensing architectures as direct consequences of the material property and loss chain constraints summarized here.

3. Chalcogenide Fiber, Waveguide, and Microcavity Platforms for MIR Sensing

Chalcogenide mid-infrared (MIR) sensing platforms have evolved from flexible fiber evanescent-wave spectroscopy (FEWS) probes to structured and functionalized fiber probes, microfibers, fiber-integrated cavities, planar waveguides, and chip-scale microcavities. The underlying sensing principle is molecular absorption in the MIR fingerprint region, but the device physics change substantially with platform geometry. In a conventional exposed fiber, the signal is mainly determined by single-pass evanescent absorption. In a microfiber, reduced diameter increases the fractional evanescent field and modifies the effective mode area. In a microcavity, the analyte can perturb resonance wavelength, linewidth, extinction ratio, or Q factor. In suspended or hollow-core waveguides, the design goal shifts toward maximizing gas–light overlap while maintaining acceptable propagation loss and mechanical stability.

This section therefore organizes chalcogenide MIR sensing platforms into three connected classes: fiber-based evanescent-wave sensing, microfiber and fiber-integrated cavity platforms, and planar waveguide or microcavity sensors. The central theme is the same across all three classes: useful MIR sensing requires a balance among optical transparency, analyte overlap, propagation or cavity loss, surface stability, sample handling, and packaging.

3.1. From Conventional FEWS to Application-Oriented Fiber Probes

The earliest chalcogenide FEWS studies established the feasibility of remote MIR chemical sensing. In 1991, Heo et al. demonstrated fiber-optic chemical sensing through evanescent-wave interaction in chalcogenide glass fibers, showing that a flexible infrared-transmitting probe could transfer chemically specific absorption information from a remote sample region [21]. In 1994, Sanghera et al. extended this concept using telluride glass fibers to record evanescent-absorption spectra of representative liquids, including water, alcohols, acetone, acetic acid, hexane, and chloroform [22]. These early studies defined the basic FEWS problem: the detected signal depends not only on glass transparency but also on interaction length, exposed geometry, surface condition, and reproducible contact between the fiber and the sample.

Early infrared glass–fiber studies then expanded FEWS from proof-of-principle chemical detection to analytical monitoring. Hocdé et al. summarized infrared–glass–fiber chemical sensing and clarified that fiber composition, probe geometry, and sample environment jointly determine spectral quality [23]. Michel et al. applied chalcogenide glass optical fibers to wastewater-pollutant analysis, demonstrating the feasibility of environmental monitoring outside a conventional FTIR cell [24]. Le Coq et al. further used infrared fibers for in situ monitoring of chemical and biochemical reactions [25]. These works

shifted chalcogenide and related infrared fibers from passive transmission media toward chemically interactive analytical probes.

Biological, biochemical and medical sensing followed from the molecular specificity of MIR absorption. Anne et al. investigated chalcogenide glass optical waveguides for infrared biosensing and linked MIR molecular fingerprints with biological sensing interfaces [26]. Lucas et al. demonstrated hydrophobic chalcogenide fibers sensitized with live cells, showing that fiber surfaces could be modified for biologically relevant MIR detection [27]. More recently, Zaiter et al. advanced this direction through biofunctionalized chalcogenide glass fibers for real-time, label-free MIR detection [28]. In parallel, Seddon proposed chalcogenide glasses as candidate materials for MIR medical endoscopy, emphasizing flexible delivery, probe miniaturization and access to biological vibrational bands [29]. Studies by Keirsse et al. further supported the translation of infrared fibers from laboratory chemical analysis to biological samples and constrained probe geometries [30,31]. In these applications, the fiber must transmit MIR light, interact with complex media, tolerate bending and handling, and remain compatible with surface functionalization, sterilization or protective packaging.

This development connects chalcogenide FEWS with waveguide-enhanced MIR chem/bio sensing, where geometry, surface chemistry and sample-interface design determine effective interaction length and detection sensitivity [32]. Yu et al. used chalcogenide films and waveguide-like sensing structures for MIR biosensing and pathogen fingerprinting, showing that engineered surfaces and enhanced local fields can improve molecular detection [33]. Houizot et al. later demonstrated looped chalcogenide fiber sensing heads, localizing the interaction region and improving the mechanical definition of the probe [34]. These studies showed that the sensing head is not a passive accessory; it determines the reproducibility of sample contact, the effective interaction length, and the baseline stability.

Rather than representing a direction that began only recently, geometry- and interface-engineered chalcogenide sensing has evolved continuously from early FEWS and functionalized fiber probes to recent tapered, side-polished, grating-assisted, ring, helical, suspended-waveguide and hollow-core platforms. Zhao et al. combined tapering with tight bending in a $Ge_{10}As_{30}Se_{38}Te_{22}$ fiber-ring sensor, showing that waist diameter, bending radius and turn number jointly determine modal displacement, interaction density, and detection performance [35]. At the chip scale, Pi et al. used suspended Ge-Sb-Se nanorib waveguides to expose a large fraction of the MIR mode directly to the surrounding gas over multiple molecular-fingerprint windows [36]. Related fiber studies quantified the influence of straight-taper geometry [37], introduced resonance-assisted long-period gratings [38], enlarged local analyte overlap through side polishing [39], extended tapered-fiber sensing using Te-containing compositions [40], and developed helical probes for compact in situ MIR analysis [41]. These advances show that useful sensitivity is obtained by co-designing the glass, modal geometry, exposed interaction length, sample interface, and package rather than by maximizing any single geometric parameter.

Figure 2 compares two geometry-engineering strategies for increasing light–analyte interaction in chalcogenide mid-infrared sensors. In the tapered $Ge_{10}As_{30}Se_{38}Te_{22}$ (GAST) fiber-ring sensor, bending displaces the guided LP_{01} field toward the outer boundary of the fiber, thereby increasing the fraction of optical energy interacting with the surrounding medium (Figure 2a). Combining a reduced bending radius with multiple turns compresses a long interaction path into a small sensing region (Figure 2b). The sensitivity and limit-of-detection data in Figure 2c show that decreasing the bending radius and increasing the number of turns generally strengthen the response. With a 50 μm waist, a 0.5 mm bending radius, and four turns, the sensor achieved a sensitivity of 1.490 ± 0.024 a.u./vol% and a limit of detection of 0.058 ± 0.001 vol% for ethanol [35].

The suspended Ge–Sb–Se nanorib waveguide extends geometry-controlled sensing from a fiber probe to a planar high-overlap platform. The CH_4 and CO_2 absorbance spectra at 3291, 4319 and 7625 nm demonstrate operation across widely separated molecular windows (Figure 2d–f). The corresponding second-harmonic (2f) wavelength-modulation signals are stronger than the free-space reference signals (Figure 2g–i), and the broadband map in Figure 2j shows how waveguides with different geometries can be assigned to different portions of the MIR fingerprint region. Together, these results show that tapering, bending, suspension and cross-sectional engineering are complementary methods for increasing modal exposure to an analyte [36].

Representative chalcogenide fiber-based evanescent-wave sensing platforms are summarized in Table 2. The key design lesson is that FEWS performance is governed by a coupled set of parameters: glass composition, exposed length, evanescent-field fraction, probe geometry, surface chemistry, sample contact, and packaging. Tapering increases evanescent-field exposure, side polishing increases local interaction area, long-period gratings introduce resonance-enhanced sensitivity, and ring or helical shaping increases interaction density within a compact fiber probe. However, all of these strategies also amplify mechanical fragility, bending loss, surface adsorption, and reproducibility challenges.

Table 2. Evolution of chalcogenide fiber-based evanescent-wave sensing platforms for MIR chemical and biological analysis.

Category	Representative Platform/Approach	Main Contribution	Main Limitation or Design Issue
Foundational FEWS and early chemical sensing	Chalcogenide and telluride glass fibers; infrared glass fiber probes	Established remote MIR chemical sensing through evanescent-wave absorption and extended FEWS from model analytes to chemical-reaction and pollutant monitoring	Single-pass absorption, limited evanescent-field fraction, surface-contact dependence, sample-matrix effects and baseline drift [21–25]
Biological, medical and functionalized FEWS	Chalcogenide fibers, infrared waveguides and surface-functionalized fiber probes	Linked MIR molecular fingerprints with biosensing, label-free surface chemistry, and potential in situ biomedical/endoscopic spectroscopy	Water absorption, nonspecific adsorption, biofouling, regeneration, sterilization, and long-term stability [26–31]
Miniaturized and localized fiber sensing heads	Looped chalcogenide fiber sensing heads and compact fiber probes	Localized the sensing region and improved probe definition for practical MIR sensing geometries	Mechanical reproducibility, fiber fragility and packaging stability [34]
Geometry-optimized tapered fibers	Ge–Sb–Se and related tapered chalcogenide fibers	Quantified how waist diameter, taper length, and transition geometry control evanescent-field exposure and sensing sensitivity	Fragility, bending loss, taper reproducibility, and handling stability [37]
Surface- and resonance-assisted fiber probes	Side-polished chalcogenide fibers and thinly clad long-period fiber gratings	Increased analyte overlap or used resonance near the phase-matching turning point to enhance refractive index or absorption sensitivity	Surface roughness, polishing-depth control, coating stability, temperature compensation, and mechanical robustness [38,39]
Long-wave and shaped fiber probes	Ge–As–Se–Te tapered fibers, tapered fiber rings and Te-based helical fibers	Extended FEWS toward longer MIR wavelengths, alcohol detection, environmental organic pollutant detection, and in situ MIR sensing	Te-rich glass processing, bending loss, mechanical stability, and reproducible sample contact [35,40,41]

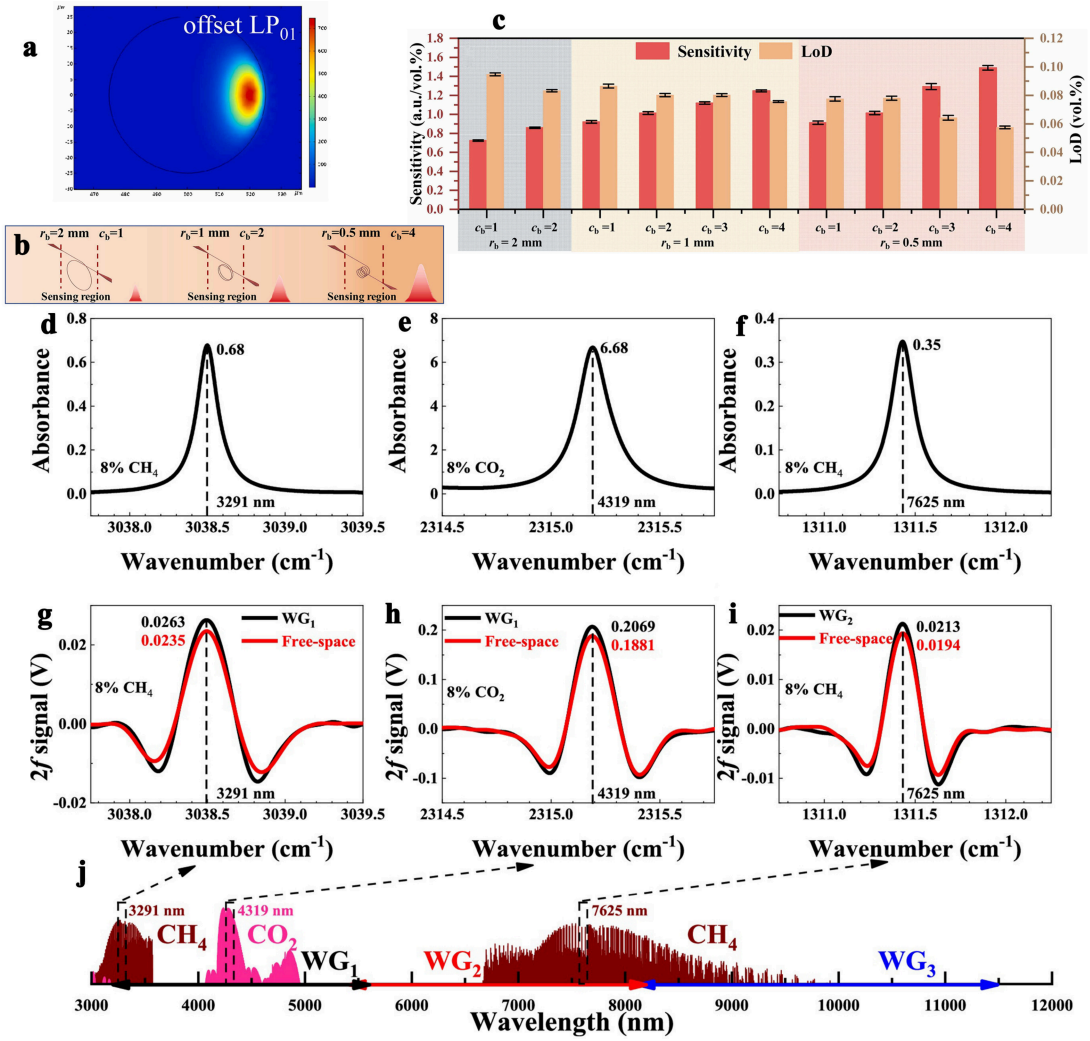

Figure 2. Geometry-engineered chalcogenide fiber and suspended-nanorib waveguide sensors for enhanced MIR light–analyte interaction. (**a**) Simulated LP_{01} mode distribution in a bent GAST fiber, showing outward displacement of the optical field. (**b**) Representative tapered fiber-ring geometries with bending radii and turn numbers of r_b = 2 mm and c_b = 1, r_b = 1 mm and c_b = 2, and r_b = 0.5 mm and c_b = 4. (**c**) Sensitivity and limit of detection of tapered fiber-ring sensors as functions of bending radius and number of turns. (**d**–**f**) Absorbance spectra of representative CH_4 and CO_2 lines at 3291, 4319, and 7625 nm. (**g**–**i**) Corresponding second-harmonic (2f) wavelength modulation signals obtained using suspended Ge–Sb–Se nanorib waveguides and free-space reference paths. (**j**) MIR absorption band map and waveguide window assignment for broadband CH_4 and CO_2 sensing using multiple suspended nanorib geometries.The dark-red and magenta regions represent the CH4 and CO2 absorption bands, respectively. Panels (**a**–**c**) are adapted with permission from Ref. [35]. Copyright © 2024 Elsevier B.V. Panels (**d**–**j**) are adapted with permission from Ref. [36]. Copyright © 2023 American Chemical Society.

3.2. Microfibers and Fiber-Integrated Cavities: Bridging FEWS Probes and Planar Resonators

Chalcogenide microfibers occupy an intermediate regime between conventional FEWS probes and lithographic planar microcavities. They preserve fiber-compatible input and output access, but their micrometer or sub-micrometer waist diameters increase the fractional evanescent field, reduce the effective mode area, and enable stronger surface interaction. This makes them attractive for both MIR sensing and nonlinear photonics. At the same time, microfibers introduce new engineering constraints: small-diameter waists are mechanically

fragile, surface contamination becomes more influential, and stable packaging is more difficult than in standard fibers.

ChG microfibers should be regarded as tunable intermediate platforms that combine strong field exposure with fiber-level accessibility, while requiring careful control of surface quality, mechanical stability, and packaging [42]. Li et al. fabricated As_2Se_3 microwires clad with polycarbonate, cyclic olefin polymer, and poly (methyl methacrylate), demonstrating that polymer cladding can improve the mechanical support and environmental robustness of chalcogenide microwires [43]. Microfiber Bragg gratings further introduce wavelength selectivity into these fiber-compatible structures. Cai et al. reported MIR microfiber Bragg gratings in As_2S_3 microfibers with a stop band near 4.5 μm, extending microfiber-grating operation toward molecularly relevant infrared wavelengths [44]. Such devices expand the functions of ChG microfibers from passive transmission and evanescent-field interaction to wavelength-selective filtering, reflection, feedback, and potentially distributed sensing.

Microfiber knot resonators introduce resonant circulation while retaining fiber compatibility. Xie et al. reported MIR chalcogenide microfiber knot resonators based on As_2S_3 microfibers [45]. Compared with straight FEWS fibers, these resonators increase the effective interaction length by allowing light to circulate around the knot. Compared with lithographic ring resonators, they preserve a flexible fiber format and do not require thin-film patterning. Their limitations arise from geometric reproducibility, mechanical stability, contact control at the coupling region, and packaging.

Figure 3 summarizes the role of ChG microfibers in this intermediate regime. Thermally drawn ChG microfibers retain transition regions connected to conventional fibers while reducing the waist to micrometer or sub-micrometer dimensions. The hybrid polymer-clad microwire and microfiber-knot examples show that ChG microfibers can be engineered into more robust or resonant structures, rather than remaining fragile exposed tapers. The calculated trends in Figure 3d–f explain why microfiber diameter is a central design variable in MIR devices. As the diameter decreases, the effective refractive index drops and the evanescent-field fraction increases, especially at longer wavelengths. This favors absorption sensing and surface interaction. However, excessive diameter reduction increases bending loss, environmental sensitivity, and susceptibility to surface contamination. The effective mode area shows a related trade-off: tapering can reduce the mode area and enhance nonlinear intensity, but overly small diameters allow the mode to expand into the surrounding medium.

Fabry–Perot fiber cavities provide another fiber-integrated resonator route. Zhang et al. demonstrated a chalcogenide Fabry–Perot fiber tunable filter using high-reflectivity coatings on chalcogenide fiber facets [46]. The device illustrates how axial optical feedback can be introduced directly in a soft-glass fiber format, making the structure relevant to MIR filtering, feedback-assisted nonlinear generation, and cavity-enhanced absorption. Its performance depends on mirror coating quality, facet flatness, finesse, thermal drift, and alignment stability.

A comparison of representative chalcogenide microfiber, grating, knot-resonator and Fabry–Perot fiber-cavity platforms is given in Table 3. These architectures bridge conventional FEWS and planar microcavities by combining flexible delivery, surface interaction, wavelength selectivity and resonant enhancement. Their strongest role is likely in hybrid MIR systems where fiber compatibility and resonant or nonlinear enhancement must coexist.

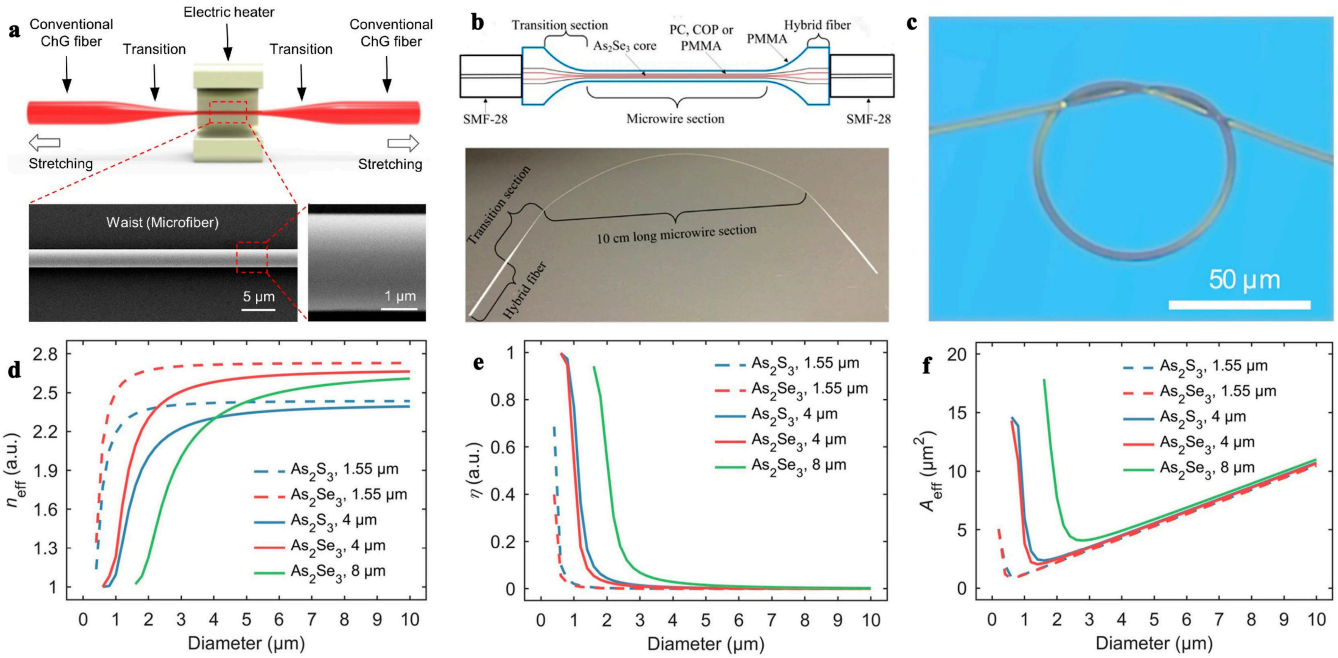

Figure 3. Chalcogenide glass microfibers as intermediate platforms between FEWS probes and integrated resonators. (**a**) Taper drawing of a chalcogenide microfiber from a conventional ChG fiber, with SEM images showing the microfiber waist and surface morphology. (**b**) Hybrid polymer-clad ChG microfiber structure and optical image of a fabricated hybrid taper. (**c**) Chalcogenide microfiber knot resonator assembled from a drawn microfiber. (**d**–**f**) Calculated diameter-dependent effective refractive index, fractional evanescent field, and effective mode area of As_2S_3 and As_2Se_3 microfibers at representative near-IR and MIR wavelengths. The figure summarizes how microfiber diameter, hybrid cladding, and resonator geometry control evanescent-field exposure, modal confinement and nonlinear interaction. Panels (**a**,**c**) are adapted with permission from Ref. [45]. Copyright © 2016 Optica Publishing Group. Panel (**b**) is adapted with permission from Ref. [43]. Copyright © 2016 Optica Publishing Group. Panels (**d**–**f**) are adapted with permission from Ref. [42].

Chalcogenide microfibers and fiber-integrated cavities are discussed here primarily as sensing and architecture platforms that bridge conventional FEWS probes and planar microcavities. Tapered microfibers increase evanescent-field exposure, Bragg gratings provide wavelength selectivity, knot resonators introduce resonant circulation, and Fabry–Perot cavities provide axial feedback. These geometries combine flexible delivery, surface interaction, spectral control and resonant enhancement, but they also increase sensitivity to fragility, surface contamination, and packaging instability. Their nonlinear-source functions are discussed separately in Section 4, where similar fiber and microwire geometries are considered from the perspective of MIR source generation rather than sensing architecture.

3.3. Planar Waveguide and Microcavity Sensors: From Resonant Enhancement to High-Overlap Gas Sensing

Planar chalcogenide waveguides and microcavities transform FEWS-like molecular interaction into lithographically controlled chip architectures. In these devices, the sensing signal is no longer limited to single-pass evanescent absorption. Straight or rib waveguides mainly measure guided-wave absorption along a defined path. Ring resonators, disks, and WGM-type cavities can convert molecular interaction into resonance shift, linewidth broadening, extinction-ratio change or Q-factor degradation. Photonic crystal cavities provide compact field localization. Suspended nanorib and hollow-core anti-resonant structures further shift the design target toward high external confinement or direct gas-core overlap.

Table 3. Representative chalcogenide microfiber and fiber-integrated cavity architectures for MIR sensing and nonlinear photonics.

Architecture	Representative Device	Function and Key Advantages	Main Limitations
Tapered microfiber	Chalcogenide glass microfiber	Enhances evanescent-field exposure and nonlinear interaction through small effective mode area and large surface-to-volume ratio	Fragile waist, surface contamination and packaging difficulty [42]
Polymer-clad microwire	PC-, COP-, or PMMA-clad As_2Se_3 microwire	Improves mechanical support and environmental protection while retaining strong optical confinement and nonlinear interaction	Polymer absorption, thermal and chemical compatibility, interface quality, and fabrication reproducibility [43]
MIR microfiber Bragg grating	As_2S_3 microfiber Bragg grating near MIR wavelengths	Combines microfiber exposure with spectral selectivity for MIR stop-band filtering and sensing	Fabrication tolerance, spectral drift and mechanical stability [44]
Microfiber knot resonator	As_2S_3 microfiber knot resonator	Introduces resonant circulation and increased interaction length while retaining a fiber-format geometry	Coupling region sensitivity and geometric reproducibility [45]
Fabry–Perot fiber cavity	Coated chalcogenide fiber segment	Provides axial feedback, tunable filtering, and a simple fiber-cavity concept	Mirror quality, facet flatness, finesse control, and thermal drift [46]

Low-loss planar chalcogenide waveguides formed the basis for integrated MIR sensing. Ma et al. reported low-loss chalcogenide waveguides for MIR chemical sensing, establishing that high-index ChG films could provide chip-scale MIR routing with losses compatible with evanescent absorption spectroscopy [47]. Zou et al. demonstrated high-index-contrast chalcogenide photonics on silicon and unconventional non-planar substrates, expanding the design space beyond standard planar chips [48]. These platforms connect FEWS-style molecular interaction with lithographically defined routing, compact footprints, and future detector or microfluidic integration.

High-Q chalcogenide resonators then enabled cavity-enhanced MIR spectroscopy. Lin et al. demonstrated high-Q chalcogenide glass-on-silicon resonators near 5.2 μm, proving that resonant enhancement could be achieved at molecularly relevant MIR wavelengths [49]. Ma et al. reported high-Q chalcogenide ring resonators for cavity-enhanced MIR spectroscopic sensing, directly linking resonator linewidth and extinction to absorption measurements [50]. Lin et al. further demonstrated CaF_2-supported high-Q chalcogenide resonators and used them for cavity-enhanced spectroscopy of ethanol solutions [51]. These studies established the basic resonator-sensing logic: increased optical path length improves sensitivity only when Q factor, analyte overlap, coupling stability, and parasitic absorption are simultaneously controlled.

Photonic crystal cavities provide a more compact field localization route. Mid-infrared waveguide photonic crystal cavities in Ge–Sb–S glass on CaF_2 substrates achieved localized resonances near 5.2 μm [52]. Although their Q factors are generally lower than those of high-Q rings or WGM-type resonators, photonic crystal cavities offer compact mode

volumes and spatially defined sensing regions. Their performance is strongly affected by fabrication disorder, sidewall roughness, dimensional tolerance and coupling design. Three-dimensional MIR photonic circuits written in chalcogenide glass also show that integration does not need to remain strictly planar [53]. Buried or three-dimensional waveguide layouts may support compact routing, interferometric sensing, astrophotonic functions or biochemical sensing geometries that are difficult to implement in two-dimensional chips.

A central lesson from chalcogenide resonator sensing is that high Q is not sufficient. For refractive index sensing, resonance shift is often the main signal. For absorption spectroscopy, linewidth broadening, Q-factor reduction, or change in resonance depth may more directly reflect molecular absorption. Useful sensing performance depends on the balance among Q factor, analyte overlap, parasitic absorption, coupling condition, thermal drift, environmental background, and detector noise. A very high-Q resonator with weak analyte overlap can underperform a moderate-Q resonator with a better sensing interface.

Recent GeSbSe waveguide and resonator platforms have moved chalcogenide sensing toward application-specific MIR circuits. Grayson et al. fabricated $Ge_{28}Sb_{12}Se_{60}$ waveguides and resonators and demonstrated on-chip MIR sensing near 3.66 μm, while also showing how process-related absorption can affect device performance [54]. Meziani et al. reported liquid and gas MIR integrated spectroscopic sensing with chalcogenide waveguides, extending integrated sensing toward longer wavelengths and more realistic sample configurations [55]. These studies mark a transition from isolated resonator demonstrations to waveguide–sensor circuits designed around target analytes, spectral windows, sample handling and packaging.

Waveguide geometry further modifies the sensing trade-off. Slot and subwavelength-grating waveguides can increase analyte overlap, but they also introduce fabrication complexity, scattering and additional loss. Comparative analysis shows that these geometries do not automatically outperform strip waveguides once practical constraints are included [56]. For chalcogenide MIR sensing, field exposure must therefore be balanced against loss, manufacturability, coupling, and environmental stability.

The suspended nanorib results highlighted in Figure 2d–j provide one of the strongest recent demonstrations of high-overlap chalcogenide gas sensing. Pi et al. demonstrated ultra-wideband $Ge_{28}Sb_{12}Se_{60}$ suspended nanorib waveguide gas sensors covering three MIR windows: 3.2–5.6 μm, 5.4–8.2 μm and 8.1–11.5 μm [36]. The key idea is that the chalcogenide rib is suspended so that a large fraction of the guided field is exposed to the surrounding gas rather than buried in a solid cladding. This geometry produced experimentally derived external confinement factors of approximately 110% and enabled ppm-level methane detection. For this review, the significance of this work lies not only in the detection limit, but also in showing that high analyte overlap, broad MIR operation, and dry-etch-free fabrication can be combined in a chalcogenide gas-sensing platform.

Hybrid hollow-core and anti-resonant waveguide designs represent another recent direction. Min et al. reported an on-chip hollow-core C_2H_2 sensor based on a hybrid chalcogenide/PDMS anti-resonant reflecting structure [57]. Although demonstrated in the near-infrared, the structure is conceptually relevant to MIR chalcogenide sensing because the gas occupies the waveguide core and directly overlaps with the optical mode rather than interacting only with an evanescent tail. This work suggests a useful future design route: chalcogenide materials can be combined with hollow-core or anti-resonant guiding to increase light–gas overlap, simplify fabrication, and reduce the conflict between strong confinement and analyte access.

Chalcogenide microcavities should also be evaluated against non-chalcogenide benchmarks. Heterogeneously integrated silicon photonics provide mature fabrication and broader photonic integration routes, while fluoride crystalline resonators provide ultra-

high-Q MIR benchmarks [58,59]. These comparisons clarify the distinctive value of chalcogenide platforms: they combine MIR transparency, high nonlinearity, high index, fiber compatibility, and thin-film processability within the same material family.

Representative planar chalcogenide waveguide and microcavity sensing platforms are summarized in Table 4. The table emphasizes how guided-wave absorption, resonant enhancement, localized field confinement, and high-overlap suspended or hollow-core geometries improve MIR molecular detection. The best MIR cavity sensor is therefore not necessarily the device with the highest Q factor but the device that produces the strongest stable molecular signal under realistic sample, coupling and packaging conditions.

Table 4. Representative planar chalcogenide waveguide and microcavity sensing architectures for MIR molecular detection.

Platform/ Architecture	Representative Device or Material	Main Sensing Mechanism	Key Advantages	Main Limitations
Planar chalcogenide waveguides	Chalcogenide strip or rib waveguides for MIR chemical sensing	Evanescent absorption along a guided path	Compact routing; chip-scale sensing; compatibility with liquid or gas samples	Propagation loss, coupling loss, interface reproducibility, and sample delivery [47,48]
Chalcogenide resonator sensors	Chalcogenide glass ring, disk or CaF_2-supported resonators	Resonance shift, linewidth change and cavity-enhanced absorption	Increased effective path length; spectral selectivity; small footprint	Q–overlap trade-off, thermal drift, coupling fluctuation, and packaging sensitivity [49–51]
Localized-field cavity sensors	Ge–Sb–S photonic-crystal cavity and related localized resonant structures	Localized resonant field enhancement	Compact mode volume; defined sensing region; strong local field	Disorder sensitivity, fabrication tolerance, and coupling complexity [52]
Non-planar or 3D-written chalcogenide circuits	Laser-written 3D MIR chalcogenide photonic circuits	Integrated routing and compact optical functions	Potential for non-planar routing and complex MIR circuits	Less mature than lithographic thin-film platforms; higher process variability [53]
Application-oriented GeSbSe waveguide sensors	$Ge_{28}Sb_{12}Se_{60}$ waveguides and resonators	On-chip MIR absorption sensing	Deeper-MIR operation; application-oriented molecular sensing	Process-related absorption, surface quality, and packaging requirements [54,55]
High-overlap gas-core or suspended structures	Suspended $Ge_{28}Sb_{12}Se_{60}$ nanorib waveguides; hybrid ChG/PDMS hollow-core ARROWs	Wideband gas absorption with high external confinement or direct gas-core overlap	Very high analyte overlap; experimentally demonstrated ECF ≈ 110%; simplified chip-scale gas-sensing concepts	Mechanical robustness, suspended-structure stability, gas packaging, calibration, and MIR translation for ARROW devices [56,57]

Overall, chalcogenide MIR sensing has progressed from fiber-delivered molecular absorption to geometry-optimized probes, microfiber resonators, and chip-scale high-overlap sensors. The field is no longer limited by whether chalcogenide glass can transmit MIR light. The decisive questions are now how the optical mode is exposed to the analyte, how parasitic absorption and scattering are suppressed, how the sample is delivered and regenerated, and how the sensing element is packaged into a stable system. This platform-level view prepares the transition to Section 4, where the same chalcogenide material advantages are used not only for sensing but also for nonlinear MIR source generation.

4. Chalcogenide Source Platforms for MIR Sensing and Nonlinear Photonics

Chalcogenide source platforms provide the source-side counterpart to MIR sensing. Molecular spectroscopy requires optical power at specific absorption bands, yet compact broadband, tunable or narrow-linewidth MIR sources remain difficult to implement. FTIR sources are broadband but bulky and relatively low-brightness, whereas quantum cascade lasers and interband cascade lasers provide strong targeted MIR emission but are less suited to broadband multi-species spectroscopy. Chalcogenide platforms address this need mainly through nonlinear optical processes, including supercontinuum generation, four-wave mixing, optical parametric conversion, Raman scattering, Brillouin scattering, and Kerr comb formation. Doped chalcogenide fibers and glass–ceramics are mentioned only briefly as related active MIR source options, because their gain mechanisms are physically distinct from the nonlinear processes emphasized in this review.

The nonlinear source functionality emphasized here arises from the same material properties that support MIR sensing: broad infrared transparency, high refractive index, large third-order nonlinearity and flexible fiber or thin-film processing. More broadly, integrated nonlinear photonics has moved from bulk and fiber geometries toward compact waveguides and resonators, where strong confinement, controllable dispersion and high optical intensity enable supercontinuum generation, frequency comb formation, wavelength conversion, optical switching, and quantum-light generation at reduced power levels [60]. For chalcogenide MIR systems, these nonlinear source routes are best discussed by source function rather than by geometry alone. Broadband supercontinuum generation, parametric conversion, Raman processes, Kerr microcombs, Brillouin lasers, and reconfigurable nonlinear resonators provide complementary routes to MIR source engineering.

In fiber platforms, source performance depends strongly on geometry. Step-index fibers emphasize transmission, power handling and fabrication simplicity. Suspended-core and photonic-crystal fibers provide smaller mode areas and stronger dispersion control. Tapered fibers and microwires further increase confinement and nonlinear efficiency, but they are more difficult to handle, package, and stabilize. The best geometry is therefore not the one with the largest nonlinear coefficient alone but the one that provides the required bandwidth, power spectral density, coherence, polarization state, and environmental robustness for a given sensing architecture.

Supercontinuum generation is the most mature nonlinear function of chalcogenide fibers. In 2012, Gattass et al. demonstrated broadband MIR generation in an all-fiber chalcogenide format [61]. In the same year, Marandi et al. reported octave-spanning MIR supercontinuum generation from 2.2 to 5 μm in a tapered As_2S_3 fiber, showing the benefit of tight confinement and dispersion engineering [62]. Suspended-core and microstructured chalcogenide fibers reported in 2013 and 2017 then provided routes to stronger nonlinear interaction, smaller effective mode area and broader control over the zero-dispersion wavelength [63,64]. These studies established chalcogenide fibers as active broadband source media rather than merely passive infrared guides.

Representative nonlinear fiber and microfiber studies further illustrate the range of achievable source functions. Petersen et al. reported a 1.4–13.3 μm supercontinuum in an ultra-high-numerical-aperture chalcogenide step-index fiber, providing one of the clearest demonstrations that chalcogenide fibers can cover multiple fundamental molecular bands [65]. Abdukerim et al. demonstrated a 2 μm Raman fiber laser based on a multimaterial chalcogenide microwire, showing that strongly confined soft-glass microwires can support narrowband Stokes-shifted emission [66]. The same group also reported a chalcogenide-based optical parametric oscillator at 2 μm, illustrating how four-wave mixing in a microwire cavity can generate tunable parametric output [67]. In parallel,

Møller et al. achieved multi-milliwatt MIR supercontinuum generation in a suspended-core chalcogenide fiber [68], and Cheng et al. extended the spectrum from 2.0 to 15.1 μm in a chalcogenide step-index fiber [69]. These works shifted the field from bandwidth demonstrations toward practical spectroscopic source development, where usable power density, coherence, linewidth, spectral flatness and stability across target bands are often more important than spectral span alone.

Reviews of MIR supercontinuum generation in chalcogenide fibers have clarified the roles of glass composition, pump wavelength, dispersion, step-index design, microstructured geometries and tapered fibers [70,71]. The broader specialty-fiber supercontinuum literature also emphasizes brightness, coherence, noise, polarization stability, and system compatibility as source metrics for spectroscopy [72]. This perspective is important because a moderately broad but stable and bright source may outperform an extremely broad but noisy spectrum in practical sensing.

Polarization and noise control have therefore become central. Ghosh et al. reported a chalcogenide-glass polarization-maintaining photonic crystal fiber for MIR supercontinuum generation, addressing the need for stable polarization during nonlinear propagation [73]. Eslami et al. reported low-noise octave-spanning MIR supercontinuum generation, highlighting relative intensity noise and coherence as key source parameters [74]. Subsequent work by Saini et al., Venck et al., and others further examined coherent and stable operation in tapered chalcogenide fibers and fiber-based MIR supercontinuum systems [75–77]. Low-loss As_2Se_3 step-index fibers and all-fiber MIR supercontinuum systems continued this transition toward practical spectroscopic modules [78,79].

Long-wavelength extension remains attractive but technically demanding. Telluride-based and long-wave selenide fibers can push supercontinuum generation deeper into the molecular fingerprint region, as shown by MIR supercontinuum generation in Te-based suspended-core chalcogenide fibers [80]. Longer-wavelength operation, however, increases sensitivity to multiphonon absorption, impurity bands, atmospheric absorption, detector limitations, and packaging materials. For sensing-oriented systems, the practical question is not the longest wavelength generated, but the usable power, stability, and calibration reliability at target molecular bands.

Four-wave mixing and optical parametric conversion provide spectrally selective alternatives to broadband supercontinuum generation. Ahmad and Rochette demonstrated a chalcogenide optical parametric oscillator based on an As_2Se_3 microwire [81] and also reported efficient broadband optical parametric four-wave mixing in chalcogenide–PMMA hybrid microwires [82]. Compared with SCG, parametric conversion is especially attractive when the analyte has known absorption bands and optical power needs to be concentrated around selected wavelengths. Raman processes provide another route to Stokes-shifted emission, while Brillouin processes can provide narrow spectral features. These functions are complementary: broadband supercontinuum sources are suited to multi-species screening, whereas Raman, Brillouin and parametric sources are better aligned with targeted or high-resolution detection.

Mid-infrared chalcogenide fiber lasers represent a related but physically distinct active-source route. Earlier work established the broader potential of MIR fiber lasers beyond the conventional silica-fiber wavelength range and demonstrated chalcogenide fiber lasing beyond 5 μm [83,84]. At the system level, Grebnev et al. emphasized that practical MIR fiber lasers and amplifiers require not only suitable gain fibers but also compatible fiber Bragg gratings, couplers, combiners, endcaps and low-loss soft-glass joining technologies [85]. Unlike SCG, FWM, Kerr-comb generation or Brillouin lasing, their MIR output originates primarily from dopant-centered stimulated emission rather than from the passive nonlinear processes emphasized above. Recent Ce^{3+}-, Tb^{3+}-, Pr^{3+}-

and Nd^{3+}-doped chalcogenide fiber lasers have extended direct fiber emission toward the 5–6 μm molecular-fingerprint region [86–91]. Transition-metal-activated chalcogenide glass-ceramics and fibers provide another related broadband-emission route, with Co/Fe-, Ni- and Co-doped systems showing broad 2.5–5.5 μm emission and potential relevance to gas-sensing source design [92–94]. These active-source studies are included here as neighboring MIR source options rather than as a separate main topic, because the focus of this review remains chalcogenide sensing platforms, nonlinear source generation and source–sensor–detector integration.

Resonator-based MIR sources provide the chip-scale counterpart to fiber and microwire sources. Recent reviews of whispering-gallery-mode microcavity lasers provide broader context for resonant source development from the visible to the mid-infrared, including concepts relevant to MIR chalcogenide microcavity platforms [95]. In chalcogenide systems, Xia et al. demonstrated engineered Raman lasing in GeSbS integrated microresonators [96] and subsequently realized microresonator soliton-comb generation on the $Ge_{25}Sb_{10}S_{65}$ integrated photonic platform [97]. The platform combines broad infrared transparency, high Kerr nonlinearity, a relatively low thermo-optic coefficient and compatibility with nanofabrication; high-Q microresonators supported both bright-soliton and dark-pulse comb states. Although these demonstrations do not directly constitute chemical sensors, they establish compact, coherent and dispersion-engineered chalcogenide source platforms whose line spacing, bandwidth and chip-scale format are relevant to future dual-comb and multi-line MIR spectroscopy.

Figure 4 compares three complementary nonlinear source functions implemented in chalcogenide fibers, microwires and microresonators. The tapered step-index fiber results in Figure 4a,b represent the broadband supercontinuum route. Experimentally, changing the pump wavelength from 2.0 to 2.6 μm substantially alters the spectral broadening, with 2.6 μm pumping producing the widest measured output. The simulations show that increasing the input peak power from 5 to 15 kW extends the long-wavelength edge of the continuum. The usable bandwidth is therefore governed jointly by pump wavelength, peak power, waveguide dispersion, and taper geometry [75]. The integrated GeSbS microresonator results in Figure 4c,d illustrate dispersion-engineered Raman dynamics. A 1.7 μm-wide resonator supports pronounced cascaded Raman lasing, whereas a 2.4 μm-wide resonator produces a broadband Raman–Kerr comb because the modified dispersion changes the phase-matching condition for four-wave mixing. Although these demonstrations operate in the near-infrared/short-wave-infrared range, they provide a clear device-level model for controlling competing Raman and Kerr processes in chalcogenide resonators and for extending integrated nonlinear sources toward longer wavelengths [96].

The microwire optical parametric oscillator in Figure 4e,f provides a spectrally selective alternative to both supercontinuum generation and Raman lasing. The COP cladding and PMMA overcoating mechanically support the As_2Se_3 microwire, while the transition sections connect the small nonlinear waist to the larger hybrid fiber. Under appropriate phase-matching and cavity-feedback conditions, the device produces narrow and tunable parametric outputs around 2 μm [67]. Figure 4 therefore presents broadband supercontinuum generation for multiband interrogation, dispersion-engineered Raman emission for Stokes-shifted output, and parametric oscillation for narrowband wavelength conversion.

The spectral reach of chalcogenide microcombs is also expanding. Multi-octave two-color soliton frequency comb generation in integrated chalcogenide microresonators extended the accessible spectral range toward the short-wave MIR [98]. Broadband MIR frequency comb design has also been explored through dispersion and mode-volume engineering [99]. These studies suggest a route from near-infrared comb technology toward molecular fingerprint spectroscopy, although long-wave MIR operation still faces

constraints from material loss, dispersion control, pump availability, detector response, and thermal stability.

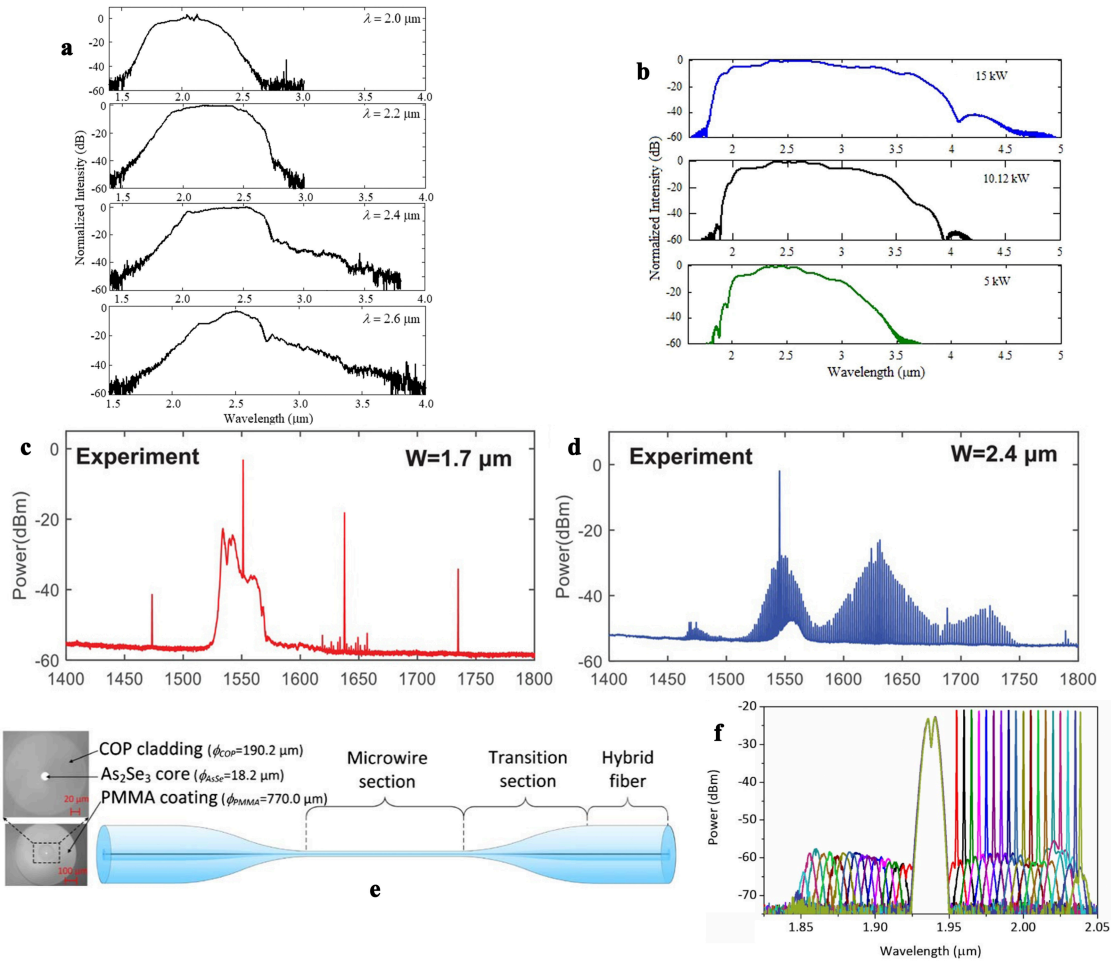

Figure 4. Chalcogenide nonlinear source routes based on tapered fibers, integrated Raman microresonators, and microwire optical parametric oscillators. (**a**) Experimentally measured supercontinuum spectra from a 3 cm tapered chalcogenide step-index fiber pumped at 2.0, 2.2, 2.4 and 2.6 μm. (**b**) Calculated supercontinuum spectra for 2.6 μm pumping at input peak powers of 5, 10.12 and 15 kW. (**c**) Experimentally measured cascaded Raman-lasing spectrum in a GeSbS microresonator with a waveguide width of 1.7 μm. (**d**) Broadband Raman–Kerr comb generated in a GeSbS microresonator with a waveguide width of 2.4 μm. (**e**) Structure of a COP-cladded As_2Se_3 microwire optical parametric oscillator, showing the hybrid-fiber, transition, and microwire sections. (**f**) Tunable optical–parametric–oscillator spectra around 2 μm. Superimposed single-pass parametric amplification spectra measured at different probe wavelengths; the different colors distinguish the individual measurement traces. Panels (**a**,**b**) are adapted from Ref. [75] under the Creative Commons Attribution 4.0 International License. Panels (**c**,**d**) are adapted from Ref. [96] under the Creative Commons Attribution 4.0 International License. Panels (**e**,**f**) are adapted with permission from Ref. [67]. Copyright © 2016 Optica Publishing Group.

Chalcogenide chip-based frequency combs are now being framed explicitly for advanced laser spectroscopy. Pan et al. reviewed $Ge_{25}Sb_{10}S_{65}$ microresonator frequency combs for spectroscopy, including bright solitons, dark pulses, Raman–Kerr combs, and broadband Kerr microcombs, as well as the future potential of MIR Kerr combs [100]. This tutorial emphasizes that chalcogenide microcombs combine high Kerr nonlinearity, lithographically controlled dispersion, and compact form factors. They are therefore attractive

for dual comb spectroscopy and molecular laser spectroscopy when spectral coverage, coherence, comb spacing, and source stability can be controlled simultaneously.

Brillouin lasing provides a narrow-linewidth source route that complements broadband supercontinuum and Kerr comb generation. Figure 5 highlights a recent ultra-high-Q on-chip chalcogenide implementation. In this device, the optical and acoustic modes are co-confined in the resonator, providing the spatial overlap and interaction time required for efficient stimulated Brillouin scattering (Figure 5a). The measured spectrum resolves cascaded even-order Stokes components up to the eighth order with a Brillouin frequency shift of 3.66 GHz (Figure 5b). The pump-dependent Stokes dynamics in Figure 5c and the wavelength-dependent second-order Stokes output in Figure 5d show that the Brillouin emission is governed by threshold behavior, resonance detuning, and the Brillouin gain bandwidth. The platform reached a Q factor of 38 million at 3.86 μm and demonstrated Brillouin lasing around 3.3 μm with a threshold of 91.9 μW [101].

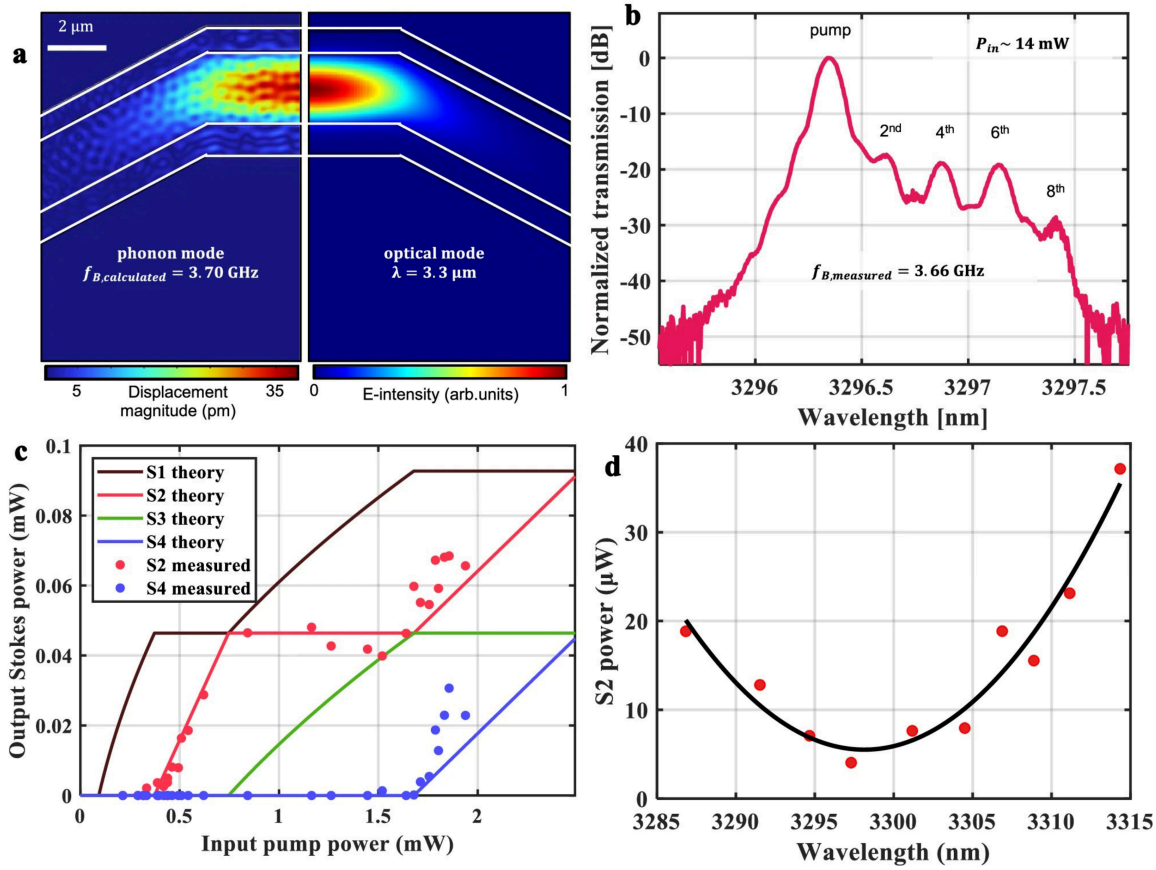

Figure 5. Mid-infrared Brillouin laser based on an ultra-high-Q on-chip chalcogenide resonator. (**a**) Simulated acoustic displacement and optical field distributions in an ultra-high-Q chalcogenide resonator operating near 3.3 μm. (**b**) Cascaded Brillouin-lasing spectrum showing even-order Stokes components and a measured Brillouin frequency shift of 3.66 GHz. (**c**) Calculated output powers of the first- to fourth-order Stokes components and measured powers of the second- and fourth-order Stokes waves as functions of input pump power. (**d**) Dependence of the second-order Stokes output power on pump wavelength. Reproduced/adapted from Ref. [101] with permission.

Chalcogenide suspended-core fibers offer an earlier fiber-based route to Brillouin source generation. A 1.5 m $As_{38}Se_{62}$ suspended-core fiber used in a ring cavity pumped near 2 μm produced a narrow Stokes line near 1.953 μm with a lasing threshold of approximately 52 mW [102]. This fiber-cavity approach uses a long interaction length and strong Brillouin gain, whereas the chip-scale resonator approach reduces footprint and threshold through

ultra-high-Q confinement. Both routes require low optical loss, strong opto-acoustic overlap, stable feedback, and robust coupling.

This comparison also reinforces the loss-chain argument discussed in Section 2. Once chalcogenide resonators approach ultra-high-Q operation, the limiting mechanisms shift from obvious fabrication defects to subtler contributions such as impurity absorption, surface-roughness scattering, surface-adsorbed molecules, cladding or substrate absorption and packaging-induced perturbations. Figure 5 shows that chalcogenide platforms can provide narrowband MIR source functions only when material purification, optical and acoustic mode design, resonator or fiber-cavity feedback, coupling and environmental stabilization are co-designed.

Ultra-high-Q chalcogenide resonators are important for both nonlinear optics and sensing. Suk et al. demonstrated on-chip chalcogenide resonators with Q factors exceeding 10 million across 3.2–4.6 μm and a peak Q of 67 million at 3.91 μm [103]. These results show that integrated chalcogenide platforms are approaching loss regimes previously associated mainly with high-quality fibers and crystalline resonators. As Q increases, the limiting factors shift from gross fabrication defects toward impurity absorption, airborne molecular absorption, surface adsorption and packaging-induced perturbations.

Post-fabrication reconfigurability addresses another bottleneck in nonlinear microcavities. Conventional dispersion engineering is fixed after fabrication, but Kerr comb generation, dispersive-wave emission, parametric oscillation, and soliton dynamics are highly sensitive to waveguide width, etch depth, sidewall angle, film thickness, and material dispersion. Lai et al. emphasized in a roadmap of integrated nonlinear chalcogenide photonics that composition, material dispersion, geometry, thermal response, and fabrication tolerance must be considered together [104]. Xia et al. then used chalcogenide photosensitivity to reconfigure dispersion itself rather than only tuning individual resonances. By optically imprinting and erasing Bragg gratings inside high-Q GeSbS microresonators, they modified mode splitting and local resonance distributions, enabling post-fabrication control of phase matching. This strategy was used to tune OPO sidebands, flatten Kerr spectra and deterministically generate compact Brillouin lasers [105].

The reconfigurable GeSbS study provides a useful organizing example because it links one photosensitive mechanism to several nonlinear source functions. Counter-propagating waves and intracavity backscattering write a Bragg grating in the microring, creating mode splitting and modifying the local dispersion landscape. The same platform can then operate in multiple nonlinear regimes, including wavelength-accurate OPO sideband tuning, spectrally flattened Kerr microcomb generation, and compact stimulated Brillouin lasing [105]. In this sense, chalcogenide photosensitivity converts dispersion from a fixed fabrication outcome into a post-fabrication programmable parameter.

Figure 6 focuses on the physical mechanism of post-fabrication dispersion reconfiguration. The SEM images in Figure 6a establish the device as a lithographically defined GeSbS microring resonator with a geometry compatible with integrated nonlinear photonics. The molecular schematics in Figure 6b connect the device-level response to the photosensitivity of GeSbS glass: optical illumination can modify local bonding configurations and therefore induce a refractive index perturbation. This material response provides the basis for writing an intracavity Bragg grating without changing the fabricated geometry.

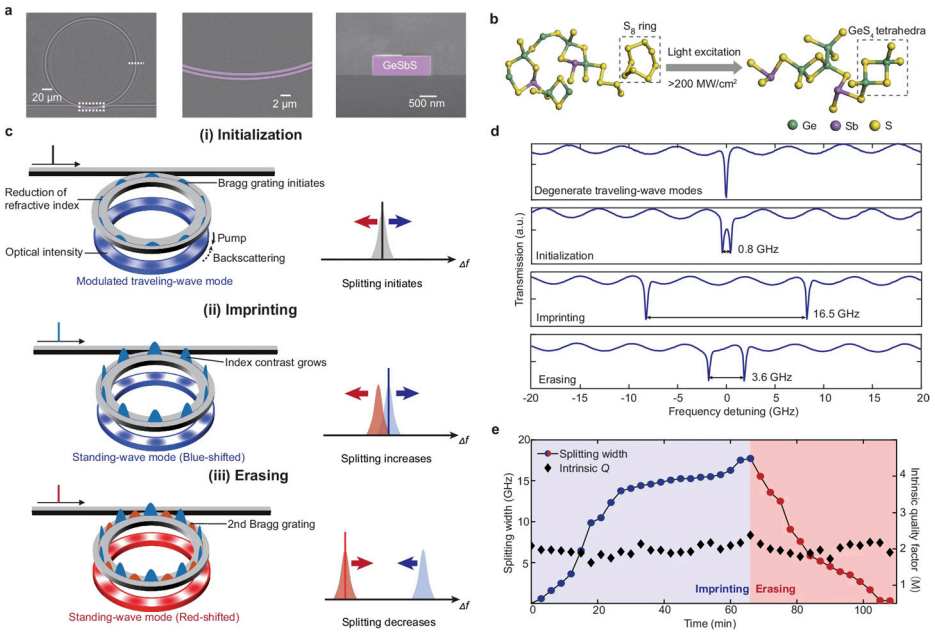

Figure 6. Reconfigurable dispersion in GeSbS chalcogenide microresonators through optically imprinted Bragg gratings. (**a**) Scanning electron microscopy images showing the structural features of the GeSbS microresonator. (**b**) Schematic molecular structures of GeSbS before and after optical illumination, illustrating the photosensitive origin of refractive-index modification. (**c**) Dispersion–configuration protocols based on initialization, grating imprinting and erasing; shaded resonant modes, pump lines, and arrows indicate mode movement during reconfiguration. (**d**) Measured microresonator transmission spectra showing tunable mode splitting during the reconfiguration process. (**e**) Measured mode splitting and intrinsic Q factor during dispersion reconfiguration. Adapted with permission from Ref. [105].

The protocol in Figure 6c explains how this photosensitivity is translated into resonator control. During initialization, weak backscattering couples clockwise and counter-clockwise traveling-wave modes. During optical imprinting, a standing-wave pattern writes a Bragg grating into the microring, producing controllable mode splitting and shifting the local resonance landscape. During erasing, the written perturbation can be weakened or reconfigured. The measured transmission spectra in Figure 6d directly verify this sequence: resonance splitting appears and evolves during imprinting, while the central frequency shifts during the process. The mode-splitting and intrinsic-Q data in Figure 6e show a key advantage of this method: the resonance landscape can be modified while maintaining high cavity quality. For nonlinear photonics, this distinction is critical because dispersion engineering is useful only if it does not destroy the low-loss resonator required for soliton formation, parametric oscillation, or Brillouin lasing.

Figure 7 shows the device-level consequence of the mechanism introduced in Figure 6. Before reconfiguration, the integrated dispersion curve in Figure 7a defines the original phase-matching landscape of the GeSbS microresonator. The corresponding microcomb spectrum in Figure 7b reflects this initial dispersion state and serves as the baseline response of the device. After multimode grating inscription, Figure 7c shows a modified integrated-dispersion profile with a flattened branch near the central pumped mode. This demonstrates that optical reconfiguration changes not only a single resonance frequency but also the local dispersion relation that governs nonlinear phase matching. The reconfigured microcomb spectrum in Figure 7d demonstrates why this capability is significant. A flatter dispersion landscape produces a more controllable and spectrally flattened comb envelope, while the simulated spectra and noise measurements support stable comb operation. For MIR sensing and spectroscopy, this is more than a microcomb optimization result. Comb

flatness, line spacing, accessible wavelength range and intensity noise determine how effectively multiple molecular absorption bands can be interrogated. Figures 6 and 7 together therefore show a transition from passive high-nonlinearity resonators to reconfigurable source platforms, where dispersion and spectral output can be adjusted after fabrication to better match pump wavelengths, molecular bands, and detector windows.

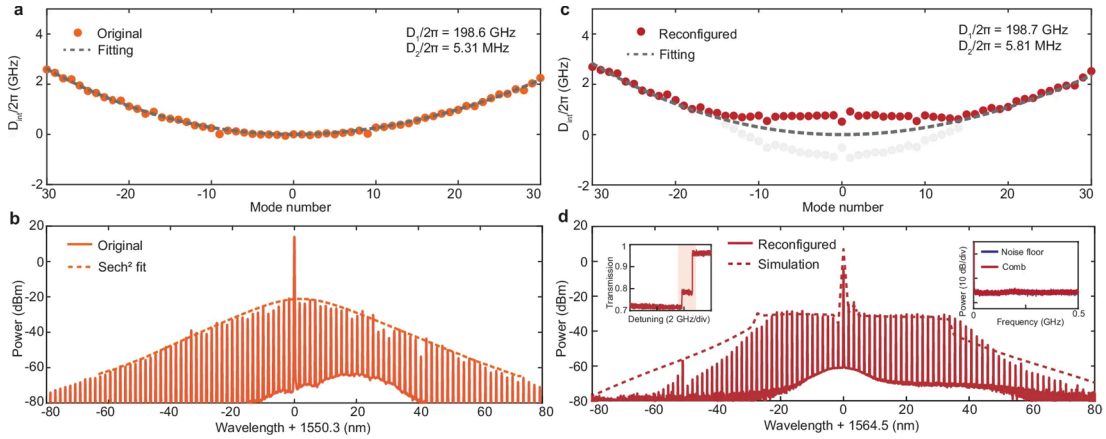

Figure 7. Spectral engineering of Kerr microcombs in reconfigured GeSbS microresonators. (**a**) Measured integrated dispersion of the original microresonator, showing the initial anomalous dispersion profile. (**b**) Kerr microcomb spectrum generated in the original dispersion state. (**c**) Measured integrated dispersion after inscription of multimode gratings, showing a flattened dispersion branch near the pumped mode. (**d**) Reconfigured Kerr microcomb spectrum with improved spectral flatness; dashed curves show simulations under similar dispersion conditions, and insets show the soliton step and radio-frequency intensity–noise spectrum. Reproduced/adapted from Ref. [105] with permission or under the applicable license.

For MIR sensing, reconfigurability is valuable because nonlinear source spectra must match molecular absorption bands, pump wavelengths, and detector windows. A fixed microresonator may generate comb lines or dispersive waves away from the desired spectral region. A reconfigurable platform could instead adapt nonlinear source functions to different analytes or measurement conditions. This capability does not eliminate the need for low loss, stable coupling, or thermal control, but it adds an important degree of freedom after fabrication.

High-Q chalcogenide microrings are also entering the quantum nonlinear landscape. Huang et al. demonstrated an integrated reconfigurable photon pair source based on spontaneous four-wave mixing in a $Ge_{25}Sb_{10}S_{65}$ microring resonator [106]. The device combined high-Q cavity enhancement, large $\chi^{(3)}$ nonlinearity, narrowband photon pair generation and photoinduced post-fabrication wavelength tuning across two free spectral ranges. Although quantum light generation is not the main focus of MIR molecular sensing, this result broadens the role of chalcogenide nonlinear microcavities from classical combs, OPOs, and Brillouin lasers toward reconfigurable integrated quantum photonics.

Despite rapid progress, nonlinear chalcogenide microcavities remain demanding. Kerr combs require controlled dispersion and stable pump detuning. Brillouin lasers require high Q, suitable optical–acoustic coupling and suppression of competing losses. MIR operation further requires control of airborne absorption, substrate loss, thermal drift, and coupling stability. For sensing systems, the key question is not only whether nonlinear oscillation occurs but whether the output is stable, spectrally matched, and compatible with detector response.

Table 5 compares representative nonlinear chalcogenide source routes by platform geometry, dominant nonlinear mechanism, source function, and remaining device-level

constraints. The table is focused on χ^3-related and cavity-enhanced nonlinear source processes, including supercontinuum generation, four-wave mixing, Raman scattering, Brillouin scattering, Kerr comb generation and reconfigurable microresonator operation. Rare earth- and transition metal-activated chalcogenide sources are discussed briefly above as neighboring active MIR source options, but they are not listed as separate main categories because their emission mechanisms are governed primarily by dopant-centered gain media photophysics rather than by the nonlinear processes emphasized here.

Table 5. Representative nonlinear chalcogenide source platforms for MIR sensing and nonlinear photonics.

Source Route	Representative Platform	Dominant Nonlinear Mechanism	Source Function	Main Design Constraints
Broadband fiber SCG	Step-index sulfide, selenide, and Te-rich chalcogenide fibers	Self-phase modulation, soliton dynamics, Raman-assisted broadening, and dispersive-wave generation	Broadband MIR or extended fingerprint-region source	Dispersion control, pump wavelength, impurity absorption, multiphonon loss, and long-wave power density [61,65,69,76–80]
Microstructured and suspended-core fiber SCG	Suspended-core and photonic crystal chalcogenide fibers	Dispersion-engineered SCG in small-mode-area fibers	Broadband and multi-milliwatt MIR source	Complex fabrication, coupling loss, structural fragility, and packaging stability [63,64,68,73]
Tapered fiber and microwire nonlinear sources	Tapered As_2S_3/As_2Se_3 fibers and hybrid microwires	SCG, FWM and optical parametric conversion	Octave-spanning MIR source or wavelength converter	Mechanical fragility, surface contamination, environmental sensitivity, and reproducible packaging [62,75,81,82]
Raman chalcogenide sources	Multi-material microwires and GeSbS integrated microresonators	Stimulated Raman scattering and Raman–Kerr dynamics	Stokes-shifted or Raman–Kerr comb source	Raman–Kerr competition, dispersion control, pump detuning and thermal stability [66,96]
Brillouin chalcogenide sources	Suspended-core chalcogenide fiber cavities and ultra-high-Q chalcogenide resonators	Stimulated Brillouin scattering	Narrow-linewidth MIR-related or MIR laser source	Optical loss, opto-acoustic overlap, cavity feedback, coupling stability, and airborne/impurity absorption [101,102]
Integrated Kerr comb and reconfigurable microresonator sources	Ge–Sb–S/Ge–Sb–Se high-Q microresonators	Kerr comb generation, soliton formation and photosensitive dispersion reconfiguration	Coherent multi-line source and post-fabrication tunable source platform	High-Q fabrication, dispersion accuracy, pump–resonance detuning, reconfiguration stability and MIR extension [97–100,103]

Nonlinear chalcogenide sources should therefore be treated as functional modules for MIR spectroscopy rather than as isolated nonlinear demonstrations. Supercontinuum fibers provide broadband coverage, parametric devices provide wavelength translation, Raman and Brillouin processes provide spectrally selective emission, Kerr microcombs provide coherent multi-line outputs, and reconfigurable resonators may allow post-fabrication matching to molecular absorption bands. Related active doped-fiber and glass-ceramic sources may supply band-specific MIR emission, but their evaluation requires a separate

gain medium framework. The value of any source route for sensing ultimately depends on spectral matching, output stability, pump compatibility, loss control, detector matching, and package robustness.

5. Integrated Source–Sensor–Detector Systems and Application-Driven Design

The preceding sections show that chalcogenide glass platforms now span flexible evanescent wave fibers, microfibers, planar waveguides, high-Q resonators, and nonlinear source devices. For MIR sensing, however, the performance of an isolated component does not determine the performance of a usable system. A broad supercontinuum spectrum is useful only if its spectral power density, noise, and detector compatibility match the target absorption bands. A high-Q cavity improves spectral resolution only when analyte overlap, coupling stability, and thermal drift are controlled. Likewise, a low-loss waveguide becomes relevant to sensing only when sample delivery, surface condition, detector response and package absorption are managed together. Chalcogenide MIR photonics should therefore be evaluated at the level of the complete source–waveguide–cavity–sensor–detector chain.

Several integration routes are emerging. One route combines nonlinear chalcogenide fiber sources with FEWS or exposed-waveguide probes. The nonlinear fiber provides broadband MIR illumination, while the sensing probe provides direct access to liquids, biological fluids, or environmental samples. This architecture is attractive for broadband molecular screening, but its sensitivity and repeatability are constrained by supercontinuum noise, detector dynamic range, water or solvent background, surface fouling, and the single-pass nature of evanescent field absorption.

A second route combines narrowband or comb-like sources with chalcogenide waveguide or microcavity sensors. QCLs, ICLs, Brillouin lasers, Kerr combs, parametric sources, and MIR fiber lasers can be matched to ring resonators, WGM-type resonators, Fabry–Perot cavities, photonic crystal cavities, suspended nanorib waveguides, or hollow-core structures. This approach is better suited to targeted gas detection, cavity-enhanced absorption, and high-resolution spectroscopy. Its main constraints are spectral alignment among the source, cavity resonance, and molecular absorption line, alongside coupling fluctuation, temperature drift, humidity, pressure variation, and gas flow stability.

A third route is fiber–chip hybrid integration. Fibers provide MIR delivery, flexible sample access, and compatibility with remote probes, whereas planar chalcogenide chips provide resonant enhancement, spectral filtering, multiplexing, and possible detector integration. This hybrid approach is likely to mature earlier than fully monolithic MIR systems because it avoids the difficulty of integrating source, waveguide, cavity, detector and sample handling on a single chip while still exploiting the strengths of both fiber and planar platforms.

Comb-assisted and broadband MIR spectroscopy provide important system-level targets for future chalcogenide platforms. MIR dual comb spectroscopy has been demonstrated using quantum-cascade laser combs, difference frequency-generated combs, electro-optic comb-based MIR systems, silicon chip-based dual comb architectures, suspended silicon nanophotonic waveguides, nanophotonic supercontinuum sources, and microcomb-based spectrometers [107–114]. Although these demonstrations are not all based on chalcogenide glasses, they define the metrics that chalcogenide sources must satisfy for spectroscopy: spectral coverage, line power, coherence, relative intensity noise, frequency calibration, detector compatibility, and long-term stability. In this context, maximum bandwidth alone is an incomplete metric. For sensing, the source should be designed around the target molecular bands, the required resolution, and the available detector response.

Sample handling is equally important. A waveguide or resonator can produce reproducible spectra only when the analyte is delivered to the optical mode under controlled and repeatable conditions. Hu et al. demonstrated this principle early by integrating a planar Ge–Sb–S chalcogenide waveguide with microfluidic channels for liquid-phase chemical sensing [115]. This example remains relevant because it connects waveguide design with sample volume, flow geometry, and solvent background. For liquid and biological sensing, future studies should report not only waveguide loss, resonance shift or absorbance but also the sample volume, flow rate, response time, recovery time, cleaning or regeneration protocol, baseline drift, and MIR compatibility of the fluidic materials.

Detector integration is another decisive part of the system. External MCT detectors remain powerful for laboratory MIR measurements, but they increase footprint, cost and, in many cases, cooling requirements. Integrated graphene, PbTe—a narrow-bandgap semiconductor, two-dimensional-material, and thermal detector—can reduce system size but introduce trade-offs in responsivity, noise-equivalent power, bandwidth, wavelength coverage, and process compatibility. Goldstein et al. demonstrated waveguide-integrated MIR photodetection using graphene on a scalable chalcogenide glass platform [116], while earlier chalcogenide glass-on-graphene photonics had already shown a route through which to combine high-index infrared waveguides with two-dimensional materials [117]. PbTe waveguide-integrated detectors and monolithic methane sensors further illustrate how chalcogenide platforms can move from passive guiding structures toward integrated readout [118,119]. More broadly, recent work on MIR optoelectronic waveguide devices based on graphene, black phosphorus, transition metal dichalcogenides, and related two-dimensional materials indicates that chalcogenide waveguides may serve as high-index field confinement platforms for active detection, modulation, or hybrid optoelectronic integration [120].

Packaging and environmental control should be considered part of the optical design rather than as a final assembly step. In ultra-high-Q chalcogenide resonators, internal impurity absorption, surface scattering, and airborne molecular absorption can all contribute appreciably to the loss budget [101,103]. In exposed-waveguide and FEWS sensors, surface adsorption, water vapor, dust, polymer absorption, adhesive absorption, and gas cell geometry can determine baseline stability. In fiber–chip systems, coupling drift and package-induced MIR absorption can dominate over the intrinsic waveguide loss. These effects are especially important because many chalcogenide devices deliberately expose a large fraction of the optical field to the surrounding medium. The same field exposure that improves sensing can also increase vulnerability to contamination, humidity, and package materials.

Application requirements therefore determine the appropriate chalcogenide architecture. Broadband multi-species spectroscopy favors stable supercontinuum or comb-assisted sources, but these sources must be judged by spectral power density, noise, coherence, and detector dynamic range. Targeted trace gas detection may be better served by QCLs, ICLs, Brillouin lasers, parametric sources, or narrowband fiber lasers, where optical power can be concentrated near selected absorption lines. Liquid sensing requires controlled sample delivery and short interaction lengths to manage water and solvent absorption. Biological sensing requires surface chemistry, antifouling strategies, sterilization compatibility and repeatable regeneration. Portable MIR sensors require robust coupling, low package absorption, and detector integration before full monolithic integration becomes realistic.

Table 6 summarizes these application-driven design rules. The comparison emphasizes that the optimal platform is not determined by chalcogenide transparency or nonlinearity alone but by the combined requirements of source selection, analyte delivery, optical overlap, detector response, drift control, calibration and packaging.

Table 6. System-level design rules for application-driven chalcogenide MIR photonic systems.

Application Target	Suitable Chalcogenide Platform	Preferred Source/Readout	Key Performance Metric	Main Bottleneck	Design Implication
Liquid chemical sensing	FEWS fiber, exposed waveguide or microfluidic ChG waveguide	FTIR, tunable MIR laser or SCG source	Baseline stability, analyte overlap, and sample volume control	Water absorption, solvent background, fouling and flow instability	Use short interaction length, controlled-flow interface and reference correction
Biological or medical sensing	Functionalized fiber, microfiber or flexible ChG probe	Broadband MIR source with differential readout	Selectivity, repeatability, probe robustness, and safety	Nonspecific adsorption, biofouling, sterilization, and biocompatibility	Combine surface functionalization with regeneration and protected probe geometry
Trace-gas sensing	Ring, WGM, Fabry–Perot cavity, suspended nanorib or hollow-core structure	QCL, ICL, Brillouin laser, Kerr comb, or narrow-linewidth MIR source	Q–overlap balance, LoD, drift and calibration stability	Humidity, pressure variation, thermal drift, gas packaging, and coupling fluctuation	Use reference resonators, temperature control and controlled gas flow
Broadband multi-species spectroscopy	Nonlinear ChG fiber, microwire or microresonator source	Stable SCG or comb-assisted spectroscopy	Spectral coverage, power spectral density, coherence and noise	Source instability, detector dynamic range and spectral calibration	Design the source around target molecular bands rather than maximum bandwidth alone
Portable fiber–chip sensing	Fiber–chip hybrid ChG platform	Compact laser, fiber SCG source or chip source with external/integrated detector	System-level SNR, footprint, robustness and coupling stability	Coupling drift, package absorption, detector noise, and alignment sensitivity	Use modular fiber–chip integration before full monolithic integration
Fully integrated MIR system	ChG waveguide, cavity, detector, and MIR-compatible package	On-chip or hybrid nonlinear source with integrated readout	Yield, reproducibility, calibration stability, and long-term baseline stability	Simultaneous integration of source, sensor, detector, sample handling, and packaging	Treat optical device, sample interface, detector, and environment as one co-designed system

Chalcogenide platforms should also be assessed against other MIR photonic materials. Silicon and germanium offer mature fabrication infrastructure and have been widely explored for MIR-integrated sensing, whereas fluoride crystalline resonators provide useful ultra-high-Q MIR benchmarks [12,58,59,121–124]. QCL-based lab-on-chip systems further demonstrate the value of matching compact MIR sources with defined sensing structures [125,126]. Suspended silicon waveguides provide another important benchmark for long-wave MIR guiding and on-chip infrared spectroscopy [127,128]. These platforms do not diminish the value of chalcogenides; instead, they clarify their strongest use cases. Chalcogenide glasses are most competitive when a system requires a combination of MIR transparency, large third-order nonlinearity, fiber compatibility, low-temperature film deposition, and hybrid integration with detectors or active materials.

The distinctive strength of chalcogenide glasses is their dual fiber–chip character. Within one material family, they can support flexible MIR fibers, exposed probes, microstructured nonlinear fibers, planar waveguides, resonators and detector-integrated hybrids. This breadth is particularly valuable for MIR sensing, where practical systems

often need both sample-accessible delivery and chip-scale enhancement or readout. In the near term, fiber–chip hybrid systems are likely to offer the most realistic path toward deployable MIR sensors. Fully integrated source–waveguide–cavity–sensor–detector systems remain a longer-term goal that will require simultaneous progress in low-loss materials, nonlinear source generation, reproducible waveguide fabrication, detector integration, MIR-compatible packaging, and calibration protocols.

Future work should therefore move beyond record-oriented component demonstrations. Materials research should continue to reduce impurity absorption, improve long-wave transparency, and stabilize thin-film processing. Device research should address Q–overlap trade-offs, dispersion control, fabrication reproducibility, and robust coupling. Sensing studies should report baseline stability, selectivity, recovery, regeneration, and performance in realistic samples. Development of nonlinear sources should be guided by molecular absorption bands and detector windows rather than by spectral span alone. Packaging, detector integration, and environmental control should be treated as core parts of chalcogenide MIR photonic design.

6. Conclusions

Chalcogenide glasses occupy a distinctive position in MIR photonics because they connect two device worlds that are often treated separately: flexible infrared fibers and chip-scale integrated photonics. Fiber platforms offer direct sample access, remote sensing capability, and nonlinear source generation, whereas thin-film waveguides and microcavities provide compact routing, resonant enhancement, dispersion control, and opportunities for detector integration. This dual fiber–chip character makes chalcogenide materials especially suitable for MIR sensing and nonlinear photonic systems.

The field has moved beyond demonstrating MIR transparency or large optical nonlinearity. In sensing, the central challenge is no longer only whether a chalcogenide fiber or waveguide can interact with an analyte, but whether the optical mode, sample interface, baseline stability, packaging and detector response can be controlled together. In nonlinear photonics, bandwidth, Q factor and conversion efficiency remain important, but practical sources must also satisfy requirements in spectral power density, noise, coherence, thermal stability and compatibility with molecular absorption bands.

Over the next 3–5 years, progress will likely depend on several device-level bottlenecks. Materials research should reduce impurity absorption, improve long-wave transparency, and stabilize sulfide, selenide, and telluride processing. Device research should focus on reproducible fabrication, Q–overlap optimization, robust coupling, dispersion control, and contamination-resistant exposed surfaces. Sensing studies should report baseline drift, selectivity, recovery, regeneration, and performance in realistic gas, liquid, or biological samples, rather than relying only on idealized demonstrations. Source development should be guided by molecular absorption bands and detector windows instead of maximum spectral span alone. In the near term, fiber–chip hybrid architectures may provide the most realistic route toward deployable MIR sensors, while fully integrated chalcogenide source–waveguide–cavity–sensor–detector systems remain a longer-term goal requiring simultaneous advances in low-loss materials, nonlinear source generation, detector integration, MIR-compatible packaging, and calibration protocols.

Author Contributions: Conceptualization, X.L.; software, C.X.; investigation, C.X.; resources, C.X.; writing—original draft preparation, X.L.; writing—review and editing, C.X. and X.L.; supervision, X.L.; project administration, X.L.; funding acquisition, X.L. All authors have read and agreed to the published version of the manuscript.

Funding: This work was supported by the National Natural Science Foundation of China (62305137).

Data Availability Statement: All data are included in the manuscript, and no additional data are required.

Conflicts of Interest: The authors declare no conflicts of interest.

References

1. Eggleton, B.J.; Luther-Davies, B.; Richardson, K. Chalcogenide photonics. *Nat. Photonics* **2011**, *5*, 141–148. [CrossRef]
2. Sanghera, J.S.; Shaw, L.B.; Aggarwal, I.D. Applications of chalcogenide glass optical fibers. *C. R. Chim.* **2002**, *5*, 873–883. [CrossRef]
3. Zakery, A.; Elliott, S.R. Optical properties and applications of chalcogenide glasses: A review. *J. Non-Cryst. Solids* **2003**, *330*, 1–12. [CrossRef]
4. Seddon, A.B. Chalcogenide glasses: A review of their preparation, properties and applications. *J. Non-Cryst. Solids* **1995**, *184*, 44–50. [CrossRef]
5. Bureau, B.; Boussard-Plédel, C.; Lucas, P.; Zhang, X.; Lucas, J. Forming glasses from Se and Te. *Molecules* **2009**, *14*, 4337–4350. [CrossRef] [PubMed]
6. Bureau, B.; Boussard-Plédel, C.; Cui, S.; Chahal, R.; Anne, M.-L.; Nazabal, V.; Zhang, X.; Lucas, J.; Lucas, P. Chalcogenide optical fibers for mid-infrared sensing. *Opt. Eng.* **2014**, *53*, 027101. [CrossRef]
7. Kadono, K. Recent progress in chalcogenide glasses applicable to infrared optical elements. *J. Ceram. Soc. Jpn.* **2022**, *130*, 595–600. [CrossRef]
8. Richardson, K.; Krol, D.; Hirao, K. Glasses for photonic applications. *Int. J. Appl. Glass Sci.* **2010**, *1*, 74–86. [CrossRef]
9. Lucas, P.; Conseil, C.; Yang, Z.; Hao, Q.; Cui, S.; Boussard-Plédel, C.; Bureau, B.; Lucas, J.; Zhang, X.-H.; Adam, J.-L.; et al. Recent progress in chalcogenide optical fibers for infrared sensing and imaging. *J. Non-Cryst. Solids* **2013**, *377*, 33–40.
10. Cui, S.; Chahal, R.; Boussard-Plédel, C.; Lucas, J.; Nazabal, V.; Zhang, X.-H.; Bureau, B. From selenium- to tellurium-based glass optical fibers for infrared spectroscopies. *Molecules* **2013**, *18*, 5373–5388. [CrossRef] [PubMed]
11. Zhang, B.; Xia, D.; Zhao, X.; Wan, L.; Li, Z. Hybrid-integrated chalcogenide photonics. *Light Adv. Manuf.* **2023**, *4*, 503–518. [CrossRef]
12. Soref, R. Mid-infrared photonics in silicon and germanium. *Nat. Photonics* **2010**, *4*, 495–497. [CrossRef]
13. Sieger, M.; Mizaikoff, B. Toward on-chip mid-infrared sensors. *Anal. Chem.* **2016**, *88*, 5562–5573. [CrossRef] [PubMed]
14. Butt, M.A. Mid-infrared photonic sensors: Exploring fundamentals, materials and integrated sensing platforms. *Sensors* **2025**, *25*, 1102. [PubMed]
15. Butt, M.A.; Pastor Abellán, D.; Piramidowicz, R. Mid-infrared integrated photonics: Material platforms and emerging applications. *Laser Photonics Rev.* **2026**, *20*, e00099. [CrossRef]
16. Mittal, V.; Mashanovich, G.Z.; Wilkinson, J.S. Perspective on thin film waveguides for on-chip mid-infrared spectroscopy of liquid biochemical analytes. *Anal. Chem.* **2020**, *92*, 1086–1094. [CrossRef] [PubMed]
17. Schädle, T.; Mizaikoff, B. Mid-infrared waveguides: A perspective. *Appl. Spectrosc.* **2016**, *70*, 1625–1638. [CrossRef] [PubMed]
18. Mizaikoff, B. Mid-IR fiber-optic sensors. *Anal. Chem.* **2003**, *75*, 258A–267A. [CrossRef] [PubMed]
19. Flores Rangel, G.; Díaz de León-Martínez, L.; Walter, L.S.; Mizaikoff, B. Recent advances and trends in mid-infrared chem/bio sensors. *TrAC Trends Anal. Chem.* **2024**, *180*, 117916. [CrossRef]
20. Petruci, J.F.S.; Sousa, D.S.; Mizaikoff, B. Advanced mid-infrared sensors for molecular analysis. *Anal. Chem.* **2025**, *97*, 6871–6890. [CrossRef] [PubMed]
21. Heo, J.; Rodrigues, M.; Saggese, S.J.; Sigel, G.H. Remote fiber-optic chemical sensing using evanescent-wave interactions in chalcogenide glass fibers. *Appl. Opt.* **1991**, *30*, 3944–3951. [CrossRef] [PubMed]
22. Sanghera, J.S.; Nguyen, V.Q.; Miklos, R.; Aggarwal, I.D. Infrared evanescent-absorption spectroscopy with chalcogenide glass fibers. *Appl. Opt.* **1994**, *33*, 6315–6322. [CrossRef] [PubMed]
23. Hocdé, S.; Boussard-Plédel, C.; Fonteneau, G.; Lucas, J. Recent developments in chemical sensing using infrared glass fibers. *J. Non-Cryst. Solids* **2000**, *274*, 17–22. [CrossRef]
24. Michel, K.; Bureau, B.; Boussard-Plédel, C.; Jouan, T.; Adam, J.L.; Staubmann, K.; Baumann, T. Monitoring of pollutant in waste water by infrared spectroscopy using chalcogenide glass optical fibers. *Sens. Actuators B Chem.* **2004**, *101*, 252–259. [CrossRef]
25. Le Coq, D.; Michel, K.; Keirsse, J.; Boussard-Plédel, C.; Fonteneau, G.; Bureau, B.; Lucas, J. Infrared glass fibers for in-situ sensing, chemical and biochemical reactions. *C. R. Chim.* **2002**, *5*, 907–913. [CrossRef]
26. Anne, M.L.; Keirsse, J.; Nazabal, V.; Hyodo, K.; Inoue, S.; Boussard-Plédel, C.; Lhermite, H.; Charrier, J.; Yanakata, K.; Loreal, O.; et al. Chalcogenide glass optical waveguides for infrared biosensing. *Sensors* **2009**, *9*, 7398–7411. [CrossRef] [PubMed]
27. Lucas, P.; Solis, M.A.; Le Coq, D.; Juncker, C.; Riley, M.R.; Collier, J.; Boesewetter, D.E.; Boussard-Plédel, C.; Bureau, B. Infrared biosensors using hydrophobic chalcogenide fibers sensitized with live cells. *Sens. Actuators B Chem.* **2006**, *119*, 355–362. [CrossRef]
28. Zaiter, R.; Adamietz, F.; Désévédavy, F.; Strutynski, C.; Bailleul, D.; Smektala, F.; Buffeteau, T.; Vellutini, L.; Dussauze, M. Biofunctionalization of chalcogenide glass fiber to enhance real time and label free detection by mid infrared spectroscopy. *Sci. Rep.* **2025**, *15*, 21679. [CrossRef] [PubMed]

29. Seddon, A.B. A prospective for new mid-infrared medical endoscopy using chalcogenide glasses. *Int. J. Appl. Glass Sci.* **2011**, *2*, 177–191. [CrossRef]
30. Keirsse, J.; Boussard-Plédel, C.; Loreal, O.; Sire, O.; Bureau, B.; Turlin, B.; Leroyer, P.; Lucas, J. Chalcogenide glass fibers used for in situ infrared spectroscopy in biology and medicine. *Proc. SPIE* **2004**, *5459*, 61–69. [CrossRef]
31. Keirsse, J.; Boussard-Plédel, C.; Fonteneau, G.; Lucas, J.; Bureau, B. Chalcogenide glass fibers for infrared spectroscopy. *Proc. SPIE* **2001**, *4566*, 78–87.
32. Mizaikoff, B. Waveguide-enhanced mid-infrared chem/bio sensors. *Chem. Soc. Rev.* **2013**, *42*, 8683–8699. [CrossRef] [PubMed]
33. Yu, C.; Ganjoo, A.; Jain, H.; Pantano, C.G.; Irudayaraj, J. Mid-IR biosensor: Detection and fingerprinting of pathogens on gold island function-alized chalcogenide films. *Anal. Chem.* **2006**, *78*, 2500–2506. [CrossRef] [PubMed]
34. Houizot, P.; Boussard-Plédel, C.; Faber, A.J.; Cheng, L.K.; Bureau, B.; Van Nijnatten, P.A.; Gielesen, W.L.M. Looped miniaturized chalcogenide fiber sensing heads for mid-infrared sensing. *Sensors* **2014**, *14*, 17905–17914. [CrossRef] [PubMed]
35. Zhao, Y.; Li, Z.; Zhao, X.; Zou, Y.; Tao, G.; Hu, W.; Yang, M.; Zhang, X.; Xu, Y. Infrared tapered fiber ring sensor for environmental detection of organic pollutants. *Sens. Actuators B Chem.* **2024**, *405*, 135361. [CrossRef]
36. Pi, M.; Zheng, C.; Zhao, H.; Peng, Z.; Guan, G.; Ji, J.; Huang, Y.; Min, Y.; Liang, L.; Song, F.; et al. Ultra-wideband mid-infrared chalcogenide suspended nanorib waveguide gas sensors with exceptionally high external confinement factor beyond free-space. *ACS Nano* **2023**, *17*, 17761–17770. [CrossRef] [PubMed]
37. Wang, M.; Yang, F.; Dai, S.; Cao, Z.; Su, J.; Ding, S.; Zhang, P. Effect of the geometries of Ge–Sb–Se chalcogenide glass tapered fiber on the sensitivity of evanescent wave sensors. *J. Light. Technol.* **2021**, *39*, 4828–4836. [CrossRef]
38. Qi, Q.; Li, Y.; Liu, T.; Zhang, P.; Dai, S.; Xu, T. Design of a coated thinly clad chalcogenide long-period fiber grating refractive index sensor based on dual-peak resonance near the phase matching turning point. *Chin. Phys. B* **2022**, *31*, 054214. [CrossRef]
39. Yang, Y.; Ge, K.; Tao, P.; Dai, S.; Wang, X.; Zhang, W.; Xu, T.; Wang, Y.; Lin, T.-J.; Zhang, P. Mid-infrared evanescent wave sensor based on side-polished chalcogenide fiber. *Ceram. Int.* **2023**, *49*, 1291–1297. [CrossRef]
40. Li, Z.; Zhao, Y.; You, T.; Zhu, J.; Xia, M.; Lu, P.; Zhang, X.; Xu, Y. Infrared evanescent wave sensing based on a $Ge_{10}As_{30}Se_{40}Te_{20}$ fiber for alcohol detection. *Sensors* **2023**, *23*, 4841. [CrossRef] [PubMed]
41. Dai, Y.; Wang, Y.; Gao, R.; Wu, Y.; Jiao, K.; Wang, R.; Li, P.; Shiryaev, V.; Wang, X. Te-based chalcogenide helical optical fiber for in-situ mid-infrared sensing. *Sens. Actuators B Chem.* **2026**, *447*, 138755. [CrossRef]
42. Cai, D.; Xie, Y.; Wang, P.; Zhang, L.; Guo, X.; Tong, L. Chalcogenide glass microfibers for mid-infrared optics. *Photonics* **2021**, *8*, 497. [CrossRef]
43. Li, L.; Al-Kadry, A.; Abdukerim, N.; Rochette, M. Design, fabrication and characterization of PC, COP and PMMA-cladded As_2Se_3 microwires. *Opt. Mater. Express* **2016**, *6*, 912–921. [CrossRef]
44. Cai, D.; Xie, Y.; Wang, P.; Zhang, L.; Guo, X.; Tong, L. Mid-infrared microfiber Bragg gratings. *Opt. Lett.* **2020**, *45*, 6114–6117. [CrossRef] [PubMed]
45. Xie, Y.; Cai, D.; Wu, H.; Wang, P.; Zhang, L.; Guo, X.; Tong, L. Mid-infrared chalcogenide microfiber knot resonators. *Photonics Res.* **2020**, *8*, 616–621. [CrossRef]
46. Zhang, K.; Peter, Y.-A.; Rochette, M. Chalcogenide Fabry–Perot fiber tunable filter. *IEEE Photonics Technol. Lett.* **2018**, *30*, 2013–2017. [CrossRef]
47. Ma, P.; Choi, D.-Y.; Yu, Y.; Gai, X.; Yang, Z.; Debbarma, S.; Madden, S.; Luther-Davies, B. Low-loss chalcogenide waveguides for chemical sensing in the mid-infrared. *Opt. Express* **2013**, *21*, 29927–29939. [CrossRef] [PubMed]
48. Zou, Y.; Zhang, D.; Lin, H.; Li, L.; Moreel, L.; Zhou, J.; Du, Q.; Ogbuu, O.; Danto, S.; Musgraves, J.D.; et al. High-performance, high-index-contrast chalcogenide glass photonics on silicon and unconventional non-planar substrates. *Adv. Opt. Mater.* **2014**, *2*, 478–486. [CrossRef]
49. Lin, H.; Li, L.; Zou, Y.; Danto, S.; Musgraves, J.D.; Richardson, K.; Kozacik, S.; Kimerling, L.C.; Agarwal, A.; Hu, J. Demonstration of high-Q mid-infrared chalcogenide glass-on-silicon resonators. *Opt. Lett.* **2013**, *38*, 1470–1472. [CrossRef] [PubMed]
50. Ma, P.; Choi, D.-Y.; Yu, Y.; Gai, X.; Yang, Z.; Debbarma, S.; Madden, S.; Luther-Davies, B. High Q factor chalcogenide ring resonators for cavity-enhanced MIR spectroscopic sensing. *Opt. Express* **2015**, *23*, 19969–19979. [CrossRef] [PubMed]
51. Lin, H.; Li, L.; Zou, Y.; Novak, S.; Richardson, K.; Hu, J. High-Q mid-infrared chalcogenide glass resonators. *Opt. Lett.* **2017**, *42*, 1476–1479.
52. Lin, H.; Li, L.; Deng, F.; Ni, C.; Danto, S.; Musgraves, J.D.; Richardson, K.; Hu, J. Demonstration of mid-infrared waveguide photonic crystal cavities. *Opt. Lett.* **2013**, *38*, 2779–2782. [CrossRef] [PubMed]
53. Rodenas, A.; Martin, G.; Arezki, B.; Psaila, N.D.; Jose, G.; Jha, A.; Labadie, L.; Kern, P.; Kar, A.K.; Thomson, R.R. Three-dimensional mid-infrared photonic circuits in chalcogenide glass. *Opt. Lett.* **2012**, *37*, 392–394. [CrossRef] [PubMed]
54. Grayson, M.; Krueper, G.; Xu, B.; Zohrabi, M.; Hjelme, D.; Gopinath, J.T.; Park, W. On-chip mid-infrared optical sensing with GeSbSe waveguides and resonators. *Opt. Express* **2023**, *31*, 877–889. [CrossRef] [PubMed]

55. Meziani, S.; Hammouti, A.; Jaafar, A.; Bodiou, L.; Lorrain, N.; Pirasteh, P.; Chahal, R.; Bénardais, A.; Courson, R.; Troles, J.; et al. Liquid and gas mid-infrared integrated spectroscopic sensor based on chal-cogenide glass waveguides. *Opt. Express* **2025**, *33*, 17002–17017. [PubMed]
56. Kita, D.M.; Michon, J.; Johnson, S.G.; Hu, J. Are slot and sub-wavelength grating waveguides better than strip waveguides for sensing? *Optica* **2018**, *5*, 1046–1054. [CrossRef]
57. Min, Y.; Pi, M.; Ma, N.; Zhang, B.; Zhang, X.; Song, F.; Wang, Y.; Li, Z.; Liang, L.; Zhang, Y.; et al. Near-infrared on-chip hol-low-core waveguide C_2H_2 sensing using hybrid chalcogenide/PDMS anti-resonant reflecting structure. *Opt. Express* **2026**, *34*, 7190–7207. [CrossRef] [PubMed]
58. Chen, Y.; Lin, H.; Hu, J.; Li, M. Heterogeneously integrated silicon photonics for the mid-infrared and spectroscopic sensing. *ACS Nano* **2014**, *8*, 6955–6961. [CrossRef] [PubMed]
59. Lecaplain, C.; Javerzac-Galy, C.; Gorodetsky, M.L.; Kippenberg, T.J. Mid-infrared ultra-high-Q resonators based on fluoride crystalline materials. *Nat. Commun.* **2016**, *7*, 13383. [CrossRef] [PubMed]
60. Geng, W.; Fang, Y.; Wang, Y.; Bao, C.; Liu, W.; Pan, Z.; Yue, Y. Nonlinear photonics on integrated platforms. *Nanophotonics* **2024**, *13*, 3253–3278. [CrossRef] [PubMed]
61. Gattass, R.R.; Shaw, L.B.; Nguyen, V.Q.; Pureza, P.C.; Aggarwal, I.D.; Sanghera, J.S. All-fiber chalcogenide-based mid-infrared supercontinuum source. *Opt. Fiber Technol.* **2012**, *18*, 345–348. [CrossRef]
62. Marandi, A.; Rudy, C.W.; Plotnichenko, V.G.; Dianov, E.M.; Vodopyanov, K.L.; Byer, R.L. Mid-infrared supercontinuum generation in tapered chalcogenide fiber for producing octave-spanning frequency comb around 3 μm. *Opt. Express* **2012**, *20*, 24218–24225. [CrossRef] [PubMed]
63. Gao, W.; El Amraoui, M.; Liao, M.; Kawashima, H.; Duan, Z.; Deng, D.; Cheng, T.; Suzuki, T.; Messaddeq, Y.; Ohishi, Y. Mid-infrared super-continuum generation in a suspended-core As_2S_3 chalcogenide microstructured optical fiber. *Opt. Express* **2013**, *21*, 9573–9583. [CrossRef] [PubMed]
64. Troles, J.; Brilland, L.; Smektala, F.; Houizot, P.; Chartier, T.; Nguyen, T.N.; Adam, J.-L. Chalcogenide microstructured fibers for infrared ap-plications. *C. R. Phys.* **2017**, *18*, 19–28.
65. Petersen, C.R.; Møller, U.; Kubat, I.; Zhou, B.; Dupont, S.; Ramsay, J.; Benson, T.; Sujecki, S.; Abdel-Moneim, N.; Tang, Z.; et al. Mid-infrared supercontinuum covering the 1.4–13.3 μm molecular fingerprint region using ultra-high NA chalcogenide step-index fibre. *Nat. Photonics* **2014**, *8*, 830–835. [CrossRef]
66. Abdukerim, N.; Li, L.; El Amraoui, M.; Messaddeq, Y.; Rochette, M. 2 μm Raman fiber laser based on a multimaterial chalcogenide microwire. *Appl. Phys. Lett.* **2017**, *110*, 161103. [CrossRef]
67. Abdukerim, N.; Li, L.; Rochette, M. Chalcogenide-based optical parametric oscillator at 2 μm. *Opt. Lett.* **2016**, *41*, 4364–4367. [CrossRef] [PubMed]
68. Møller, U.; Yu, Y.; Kubat, I.; Petersen, C.R.; Gai, X.; Brilland, L.; Méchin, D.; Caillaud, C.; Troles, J.; Luther-Davies, B.; et al. Multi-milliwatt mid-infrared supercontinuum generation in a suspended core chalcogenide fiber. *Opt. Express* **2015**, *23*, 3282–3291. [CrossRef] [PubMed]
69. Cheng, T.; Nagasaka, K.; Tuan, T.H.; Xue, X.; Matsumoto, M.; Tezuka, H.; Suzuki, T.; Ohishi, Y. Mid-infrared supercontinuum generation spanning 2.0 to 15.1 μm in a chalcogenide step-index fiber. *Opt. Lett.* **2016**, *41*, 2117–2120. [CrossRef] [PubMed]
70. Dai, S.; Wang, Y.; Peng, X.; Zhang, P.; Wang, X. A review of mid-infrared supercontinuum generation in chalcogenide fibers. *Appl. Sci.* **2018**, *8*, 707. [CrossRef]
71. Wang, Y.; Dai, S. Mid-infrared supercontinuum generation in chalcogenide glass fibers: A brief review. *PhotoniX* **2021**, *2*, 9. [CrossRef]
72. Sylvestre, T.; Genier, E.; Ghosh, A.N.; Bowen, P.; Genty, G.; Troles, J.; Mussot, A.; Peacock, A.C.; Klimczak, M.; Heidt, A.M.; et al. Recent advances in supercontinuum generation in specialty optical fibers. *J. Opt. Soc. Am. B* **2021**, *38*, F90–F103. [CrossRef]
73. Ghosh, A.N.; Meneghetti, M.; Petersen, C.R.; Bang, O.; Brilland, L.; Venck, S.; Troles, J.; Dudley, J.M.; Sylvestre, T. Chalcogenide-glass polar-ization-maintaining photonic crystal fiber for mid-infrared supercontinuum generation. *J. Phys. Photonics* **2019**, *1*, 044003. [CrossRef]
74. Eslami, Z.; Ryczkowski, P.; Närhi, M.; Genty, G.; Toivonen, J.; Dudley, J.M. Low-noise octave-spanning mid-infrared supercontinuum generation in a multimode chalcogenide fiber. *Opt. Lett.* **2020**, *45*, 3103–3106. [CrossRef] [PubMed]
75. Saini, T.S.; Tuan, T.H.; Suzuki, T.; Ohishi, Y. Coherent mid-IR supercontinuum generation using tapered chalcogenide step-index optical fiber: Experiment and modelling. *Sci. Rep.* **2020**, *10*, 2236. [CrossRef] [PubMed]
76. Lemière, A.; Bizot, R.; Désévédavy, F.; Gadret, G.; Jules, J.-C.; Mathey, P.; Aquilina, C.; Béjot, P.; Billard, F.; Faucher, O.; et al. 1.7–18 μm mid-infrared supercontinuum generation in a dispersion-engineered step-index chalcogenide fiber. *Results Phys.* **2021**, *26*, 104397. [CrossRef]
77. Venck, S.; St-Hilaire, A.; Brilland, L.; Désévédavy, F.; Caillaud, C.; Toupin, P.; Troles, J.; Smektala, F.; Vallée, R.; Bernier, M. 2–10 μm mid-infrared fiber-based supercontinuum laser source: Experiment and simulation. *Laser Photonics Rev.* **2020**, *14*, 2000011. [CrossRef]

78. Robichaud, L.-R.; Fortin, V.; Gauthier, J.-C.; Chatigny, S.; Couillard, J.-F.; Delarosbil, J.-L.; Vallée, R.; Bernier, M. Compact 3–8 μm supercon-tinuum generation in a low-loss As_2Se_3 step-index fiber. *Opt. Lett.* **2016**, *41*, 4605–4608. [CrossRef] [PubMed]
79. Hudson, D.D.; Antipov, S.; Li, L.; Alamgir, I.; Hu, T.; El Amraoui, M.; Messaddeq, Y.; Rochette, M.; Jackson, S.D.; Fuerbach, A.; et al. Toward all-fiber supercontinuum spanning the mid-infrared. *Optica* **2017**, *4*, 1163–1166. [CrossRef]
80. Wu, B.; Zhao, Z.; Wang, X.; Tian, Y.; Mi, N.; Chen, P.; Xue, Z.; Liu, Z.; Zhang, P.; Shen, X.; et al. Mid-infrared supercontinuum generation in a suspended-core tellurium-based chalcogenide fiber. *Opt. Mater. Express* **2018**, *8*, 1341–1348. [CrossRef]
81. Ahmad, R.; Rochette, M. Chalcogenide optical parametric oscillator. *Opt. Express* **2012**, *20*, 10095–10100. [CrossRef] [PubMed]
82. Ahmad, R.; Rochette, M. Efficient and broadband optical parametric four-wave mixing in chalcogenide–PMMA hybrid microwires. *Opt. Express* **2012**, *20*, 9572–9580. [CrossRef] [PubMed]
83. Jackson, S.D. Towards high-power mid-infrared emission from a fibre laser. *Nat. Photonics* **2012**, *6*, 423–431. [CrossRef]
84. Nunes, J.J.; Sojka, Ł.; Crane, R.W.; Furniss, D.; Tang, Z.Q.; Mabwa, D.; Xiao, B.; Benson, T.M.; Farries, M.; Kalfagiannis, N.; et al. Room temperature mid-infrared fiber lasing beyond 5 μm in chalcogenide glass small-core step index fiber. *Opt. Lett.* **2021**, *46*, 3504–3507. [CrossRef] [PubMed]
85. Grebnev, K.; Perminov, B.; Fernandez, T.T.; Fuerbach, A.; Chernysheva, M. Fluoride and chalcogenide glass fiber components for mid-infrared lasers and amplifiers: Breakthroughs, challenges, and future perspective. *APL Photonics* **2024**, *9*, 110901. [CrossRef]
86. Koltashev, V.V.; Frolov, M.P.; Leonov, S.O.; Sverchkov, S.E.; Galagan, B.I.; Korostelin, Y.V.; Skasyrsky, Y.K.; Snopatin, G.E.; Sukhanov, M.V.; Velmuzhov, A.P.; et al. 5 μm CW Ce^{3+}-doped chalcogenide glass fiber laser with 17% slope efficiency. *Opt. Lett.* **2024**, *49*, 2737–2740. [CrossRef] [PubMed]
87. Koltashev, V.V.; Denker, B.I.; Galagan, B.I.; Snopatin, G.E.; Sukhanov, M.V.; Sverchkov, S.E.; Velmuzhov, A.P.; Plotnichenko, V.G. 150 mW Tb^{3+}-doped chalcogenide glass fiber laser emitting at $\lambda > 5$ μm. *Opt. Laser Technol.* **2023**, *161*, 109233. [CrossRef]
88. Sukhanov, M.V.; Lashmanov, E.N.; Kotereva, T.V.; Velmuzhov, A.P.; Shiryaev, V.S. Continuous 5.22–5.31 μm wavelength lasing in optical fiber based on Tb^{3+}-doped gallium-free selenide glass. *Opt. Mater.* **2025**, *167*, 117314. [CrossRef]
89. Kotereva, T.V.; Sukhanov, M.V.; Lashmanov, E.N.; Velmuzhov, A.P.; Shiryaev, V.S. Continuous Pr^{3+}-doped chalcogenide glass fiber laser emit-ting in the 5.60–5.83 μm range. *Opt. Mater.* **2025**, *168*, 117528. [CrossRef]
90. Frolov, M.P.; Denker, B.I.; Galagan, B.I.; Koltashev, V.V.; Plotnichenko, V.G.; Sukhanov, M.V.; Sverchkov, S.E.; Velmuzhov, A.P. Cross-relaxation processes in Nd-doped selenide glass and 5.7 μm laser action in it. *J. Lumin.* **2025**, *280*, 121089. [CrossRef]
91. Koltashev, V.V.; Pushkin, A.V.; Sukhanov, M.V.; Velmuzhov, A.P.; Sverchkov, S.E.; Galagan, B.I.; Denker, B.I.; Frolov, M.P.; Potemkin, F.V.; Plotnichenko, V.G. 100 mW mid-infrared Ce^{3+}-doped chalcogenide fiber laser. *Opt. Fiber Technol.* **2026**, *98*, 104524. [CrossRef]
92. Lu, X.; Li, J.; Yang, L.; Ren, J.; Sun, M.; Yang, A.; Yang, Z.; Jain, R.K.; Wang, P. Broadband mid-infrared (2.5–5.5 μm) emission from Co^{2+}/Fe^{2+} codoped chalcogenide glass ceramics. *Opt. Lett.* **2020**, *45*, 2676–2679. [CrossRef] [PubMed]
93. Lu, X.; Liu, H.; Tian, K.; Yang, A.; Liu, Z.; Shen, X.; Yang, Z.; Ren, J.; Wang, P.; Yang, Z. Mid-infrared 3–4 μm emission of Ni^{2+} doped chalco-genide glass-ceramic fiber. *Ceram. Int.* **2023**, *49*, 13386–13391. [CrossRef]
94. Liu, H.; Gao, Y.; Jiang, Y.; Lu, X.; Yang, Z.; Wang, P.; Yang, Z. Ultrabroadband mid-infrared emission and gas sensing of cobalt-doped chalco-genide glass ceramics. *Opt. Lett.* **2024**, *49*, 5807–5810. [CrossRef] [PubMed]
95. Li, A.; Zhang, Y.; Lu, X. Whispering-Gallery-Mode microcavity lasers from visible to mid-infrared: Applications. *Photonics* **2026**, *13*, 174. [CrossRef]
96. Xia, D.; Huang, Y.; Zhang, B.; Zeng, P.; Zhao, J.; Yang, Z.; Sun, S.; Luo, L.; Hu, G.; Liu, D.; et al. Engineered Raman lasing in photonic integrated chalcogenide microresonators. *Laser Photonics Rev.* **2022**, *16*, 2100443. [CrossRef]
97. Xia, D.; Yang, Z.; Zeng, P.; Zhang, B.; Wu, J.; Wang, Z.; Zhao, J.; Gao, M.; Huang, Y.; Huang, J.; et al. Integrated chalcogenide photonics for microresonator soliton combs. *Laser Photonics Rev.* **2023**, *17*, 2200219. [CrossRef]
98. Cheng, H.; Lin, G.; Xia, D.; Luo, L.; Lu, S.; Yu, C.; Zhang, B. Multi-octave two-color soliton frequency comb in integrated chalcogenide micro-resonators. *Front. Optoelectron.* **2024**, *17*, 36. [CrossRef] [PubMed]
99. Lu, S.; Lin, G.; Xia, D.; Wang, Z.; Luo, L.; Li, Z.; Zhang, B. Broadband mid-infrared frequency comb in integrated chalcogenide microresonator. *Photonics* **2023**, *10*, 628. [CrossRef]
100. Pan, J.; Xia, D.; Wang, Z.; Zhang, B.; Li, Z. Chalcogenide chip-based frequency combs for advanced laser spectroscopy. *J. Light. Technol.* **2023**, *41*, 4065–4077. [CrossRef]
101. Ko, K.; Suk, D.; Kim, D.; Park, S.; Sen, B.; Kim, D.-G.; Wang, Y.; Dai, S.; Wang, X.; Wang, R.; et al. A mid-infrared Brillouin laser using ultra-high-Q on-chip resonators. *Nat. Commun.* **2025**, *16*, 2707. [CrossRef] [PubMed]
102. Hu, K.; Kabakova, I.V.; Büttner, T.F.S.; Lefrancois, S.; Hudson, D.D.; He, S.; Eggleton, B.J. Low-threshold Brillouin laser at 2 μm based on suspended-core chalcogenide fiber. *Opt. Lett.* **2014**, *39*, 4651–4654. [CrossRef] [PubMed]
103. Suk, D.; Ko, K.; Wang, R.; Wang, X.; Choi, D.-Y.; Lee, H. Ultra-high-Q chalcogenide glass on-chip resonators attaining internal impurity-limited loss in the mid-infrared. *Opt. Express* **2025**, *33*, 32033–32045. [CrossRef] [PubMed]

104. Lai, C.K.; Bui, C.T.; Russell, R.L.; Casas Bedoya, A.; Choi, D.-Y.; Madden, S.J.; Merklein, M.; Eggleton, B.J. Integrated nonlinear photonics with chalcogenide glasses: Compositions, properties, applications, and roadmap. *Opt. Mater. Express* **2025**, *15*, 3210–3241. [CrossRef]
105. Xia, D.; Luo, L.; Wang, L.; Zhao, X.; Yang, Z.; Wu, J.; Yang, Q.-F.; Li, Z.; Zhang, B. Reconfigurable chalcogenide integrated nonlinear photonics. *Nat. Commun.* **2025**, *16*, 10133. [CrossRef] [PubMed]
106. Huang, P.; Chen, B.; Xia, D.; Li, Z.; Zhang, B.; Liu, Z.; Wei, D.; Li, Z.; Liu, J. Integrated reconfigurable photon-pair source based on high-Q nonlinear chalcogenide glass microring resonators. *Nano Lett.* **2023**, *23*, 4487–4494. [CrossRef] [PubMed]
107. Villares, G.; Hugi, A.; Blaser, S.; Faist, J. Dual-comb spectroscopy based on quantum-cascade-laser frequency combs. *Nat. Commun.* **2014**, *5*, 5192. [CrossRef] [PubMed]
108. Villares, G.; Wolf, J.; Kazakov, D.; Süess, M.J.; Hugi, A.; Beck, M.; Faist, J. On-chip dual-comb based on quantum cascade laser frequency combs. *Appl. Phys. Lett.* **2015**, *107*, 251104. [CrossRef]
109. Cruz, F.C.; Maser, D.L.; Johnson, T.; Ycas, G.; Klose, A.; Giorgetta, F.R.; Coddington, I.; Diddams, S.A. Mid-infrared optical frequency combs based on difference frequency generation for molecular spectroscopy. *Opt. Express* **2015**, *23*, 26814–26824. [CrossRef] [PubMed]
110. Yan, M.; Luo, P.-L.; Iwakuni, K.; Millot, G.; Hänsch, T.W.; Picqué, N. Mid-infrared dual-comb spectroscopy with electro-optic modulators. *Light Sci. Appl.* **2017**, *6*, e17076. [CrossRef] [PubMed]
111. Yu, M.; Okawachi, Y.; Griffith, A.G.; Picqué, N.; Lipson, M.; Gaeta, A.L. Silicon-chip-based mid-infrared dual-comb spectroscopy. *Nat. Commun.* **2018**, *9*, 1869. [CrossRef] [PubMed]
112. Nader, N.; Kowligy, A.; Chiles, J.; Stanton, E.J.; Timmers, H.; Lind, A.J.; Cruz, F.C.; Lesko, D.M.; Briggman, K.A.; Nam, S.W.; et al. Infrared frequency comb generation and spectroscopy with suspended silicon nanophotonic waveguides. *Optica* **2019**, *6*, 1269–1276. [CrossRef]
113. Guo, H.; Weng, W.; Liu, J.; Yang, F.; Hänsel, W.; Brès, C.S.; Thévenaz, L.; Holzwarth, R.; Kippenberg, T.J. Nanophotonic supercontinuum-based mid-infrared dual-comb spectroscopy. *Optica* **2020**, *7*, 1181–1188. [CrossRef]
114. Bao, C.; Suh, M.-G.; Vahala, K. Architecture for microcomb-based GHz-mid-infrared dual-comb spectroscopy. *Nat. Commun.* **2021**, *12*, 6573. [CrossRef] [PubMed]
115. Hu, J.; Tarasov, V.; Agarwal, A.; Kimerling, L.; Carlie, N.; Petit, L.; Richardson, K. Fabrication and testing of planar chalcogenide waveguide integrated microfluidic sensor. *Opt. Express* **2007**, *15*, 2307–2314. [CrossRef] [PubMed]
116. Goldstein, J.; Lin, H.; Deckoff-Jones, S.; Hempel, M.; Lu, A.-Y.; Richardson, K.A.; Palacios, T.; Kong, J.; Hu, J.; Englund, D. Wave-guide-integrated mid-infrared photodetection using graphene on a scalable chalcogenide glass platform. *Nat. Commun.* **2022**, *13*, 3914. [CrossRef] [PubMed]
117. Lin, H.; Song, Y.; Huang, Y.; Kita, D.; Deckoff-Jones, S.; Wang, K.; Li, L.; Li, J.; Zheng, H.; Luo, Z.; et al. Chalcogenide glass-on-graphene photonics. *Nat. Photonics* **2017**, *11*, 798–805. [CrossRef]
118. Han, Z.; Singh, V.; Kita, D.; Monmeyran, C.; Becla, P.; Su, P.; Li, J.; Huang, X.; Kimerling, L.C.; Hu, J.; et al. On-chip chalcogenide glass waveguide-integrated mid-infrared PbTe detectors. *Appl. Phys. Lett.* **2016**, *109*, 071111. [CrossRef]
119. Su, P.; Han, Z.; Kita, D.; Becla, P.; Lin, H.; Deckoff-Jones, S.; Richardson, K.; Kimerling, L.C.; Hu, J.; Agarwal, A. Monolithic on-chip mid-IR methane gas sensor with waveguide-integrated detector. *Appl. Phys. Lett.* **2019**, *114*, 051103. [CrossRef]
120. Qi, L.; Xu, T.; Xing, Z.; Chen, S.; Zhang, Z.; Liu, T.; Cheng, Z. Mid-infrared optoelectronic waveguide devices with 2D materials. *Adv. Phys. Res.* **2025**, *4*, 2400079. [CrossRef]
121. Lin, P.T.; Singh, V.; Hu, J.; Richardson, K.; Musgraves, J.D.; Luzinov, I.; Hensley, J.; Kimerling, L.C.; Agarwal, A. Chip-scale mid-infrared chemical sensors using air-clad pedestal silicon waveguides. *Lab Chip* **2013**, *13*, 2161–2166. [CrossRef] [PubMed]
122. Singh, V.; Lin, P.T.; Patel, N.; Lin, H.; Li, L.; Zou, Y.; Deng, F.; Ni, C.; Hu, J.; Giammarco, J.; et al. Mid-infrared materials and devices on a Si platform for optical sensing. *Sci. Technol. Adv. Mater.* **2014**, *15*, 014603. [CrossRef] [PubMed]
123. Lin, H.; Luo, Z.; Gu, T.; Kimerling, L.C.; Wada, K.; Agarwal, A.; Hu, J. Mid-infrared integrated photonics on silicon: A perspective. *Nanophotonics* **2018**, *7*, 393–420. [CrossRef]
124. Hu, T.; Dong, B.; Luo, X.; Liow, T.-Y.; Song, J.; Lee, C.; Lo, G.-Q. Silicon photonic platforms for mid-infrared applications. *Photonics Res.* **2017**, *5*, 417–430. [CrossRef]
125. Charlton, C.; Giovannini, M.; Faist, J.; Mizaikoff, B. Low-power sensor for measurement of trace gases using quantum cascade lasers. *Anal. Chem.* **2006**, *78*, 4224–4227. [PubMed]
126. Schwarz, B.; Reininger, P.; Ristanic, D.; Detz, H.; Andrews, A.M.; Schrenk, W.; Strasser, G. Monolithically integrated mid-infrared lab-on-a-chip using plasmonics and quantum cascade structures. *Nat. Commun.* **2014**, *5*, 4085. [CrossRef] [PubMed]

127. Kita, D.M.; Lin, H.; Agarwal, A.; Richardson, K.; Luzinov, I.; Gu, T.; Hu, J. On-chip infrared spectroscopic sensing: Redefining the benefits of scaling. *IEEE J. Sel. Top. Quantum Electron.* **2017**, *23*, 5900110. [CrossRef]
128. Penadés, J.S.; Ortega-Moñux, A.; Nedeljkovic, M.; Halir, R.; Khokhar, A.Z.; Alonso-Ramos, C.; Qu, Z.; Molina-Fernández, Í.; Cheben, P.; Mashanovich, G.Z. Suspended silicon waveguides for long-wave infrared wavelengths. *Opt. Lett.* **2018**, *43*, 795–798. [CrossRef] [PubMed]